Research Paper

GEOSPHERE

GEOSPHERE, v. 15

https://doi.org/10.1130/GES02054.1

17 figures; 3 tables; 1 set of supplemental files

CORRESPONDENCE: haproffp@uncw.edu

CITATION: Haproff, P.J., Zuza, A.V., Yin, A., Harrison, T.M., Manning, C.E., Dubey, C.S., Ding, L., Wu, C., and Chen, J.L., 2019, Geologic framework of the northern Indo-Burma Ranges and lateral correlation of Himalayan-Tibetan lithologic units across the eastern Himalayan syntaxis: Geosphere, v. 15, https://doi.org/10.1130/GES02054.1.

Science Editor: Raymond M. Russo

Received 17 August 2018
Revision received 19 December 2018
Accepted 27 February 2019

Geologic framework of the northern Indo-Burma Ranges and lateral correlation of Himalayan-Tibetan lithologic units across the eastern Himalayan syntaxis

Peter J. Haproff[1,2], Andrew V. Zuza[3], An Yin[2], T. Mark Harrison[2], Craig E. Manning[2], Chandra S. Dubey[4], Lin Ding[5], Chen Wu[6], and Jianlin Chen[7]

[1]Department of Earth and Ocean Sciences, University of North Carolina, Wilmington, North Carolina 28403, USA
[2]Department of Earth, Planetary, and Space Sciences, University of California, Los Angeles, California 90095, USA
[3]Nevada Bureau of Mines and Geology, University of Nevada, Reno, Nevada 89557, USA
[4]Department of Geology, Delhi University, Delhi 110007, India
[5]Institute of Tibetan Plateau Research, Chinese Academy of Sciences, Beijing 100101, China
[6]Structural Geology Group, China University of Geosciences, Beijing 100083, China
[7]State Key Laboratory of Isotope Geochemistry, Guangzhou Institute of Geochemistry, Chinese Academy of Sciences, Guangzhou 510640, China

ABSTRACT

The Cenozoic India-Asia collision generated both the east-trending Himalayan orogen and the north-trending *Eastern* and *Western Flanking Belts* located along the margins of the Indian subcontinent. Although the tectonic development of both flanking belts is key to understanding mechanisms of continental deformation during indenter-induced collision, few field-based studies coupled with geochronological and geochemical methods have been applied to these tectonic domains. In this study, we investigate the lateral correlation of lithologic units between the northern Indo-Burma Ranges, the northernmost segment of the Eastern Flanking Belt, and the eastern Himalayan-Tibetan orogen by integrating field observations, U-Pb zircon geochronology, and whole-rock geochemistry. Our findings provide new quantitative constraints to interpretations that the northern Indo-Burma Ranges expose the eastward continuation of several lithologic units of the Himalayan orogen and Lhasa terrane. Our field work documents a stack of thrust-bounded lithologic units present in the study area. The northernmost and structurally highest Lohit Plutonic Complex consists of Mesoproterozoic basement rocks (ca. 1286 Ma) and Late Jurassic–Cretaceous granitoids (ca. 156–69 Ma) with positive ε_{Nd} values and initial $^{87}Sr/^{86}Sr$ ratios of ~0.705, which are correlative to the Bomi-Chayu complex and the northern Gangdese batholith, respectively. The structurally lower Tidding-Mayodia mélange complex, composed of basalt, gabbro, ultramafic rocks, and mafic schist of a dismembered ophiolite sequence, is interpreted in this study as the eastward extension of the Indus-Yarlung suture zone. Structurally below the suture zone are the Mayodia gneiss and Lalpani schist, which are interpreted to correlate with the Lesser Himalayan Sequence based on comparable metamorphic lithologies, negative ε_{Nd} values, and similar Mesoproterozoic–Cambrian detrital zircon age spectra. In contrast to the above metamorphic units, the structurally lowest Tezu unit consists of siliciclastic strata that may be correlated with the Miocene–Pliocene Siwalik Group of the Himalayan orogen. Despite the above correlations, notable Himalayan-Tibetan lithologic units are absent in the northern Indo-Burma Ranges, including the Mesozoic–Cenozoic southern Gangdese batholith belt and its cover sequence of the Linzizong volcanic rocks, Xigaze forearc basin, Tethyan Himalayan Sequence, and Greater Himalayan Crystalline Complex of south-central Tibet and the central Himalaya. We interpret the absence of these lithologic units to be a result of a greater magnitude of crustal shortening and/or underthrusting of the Indian cratonal rocks than that across the Himalayan orogen to the west. This interpretation is supported by a southward decrease in the map-view distance between the active range-bounding thrust and the Indus-Yarlung suture zone in the northern Indo-Burma Ranges, from ~200 km in the north near the eastern Himalayan syntaxis to ~5 km in the south across a distance of ~200–300 km.

INTRODUCTION

The Cenozoic India-Asia collision generated the Himalayan collisional system, which consists of the convergence-perpendicular Himalayan orogen and convergence-parallel flanking belts located along the eastern and western margins of the Indian subcontinent (Gansser, 1964; Yin, 2006) (Fig. 1A). Although the geology and tectonic evolution of the Himalayan orogen are well documented (Le Fort, 1975; Le Fort, 1996; DeCelles et al., 2000, 2001; Hodges, 2000; Yin and Harrison, 2000; Yin, 2006, 2010; Webb et al., 2013, 2017), relatively few geologic studies have focused on the flanking belts (cf. Tapponnier et al., 1981; Ni et al., 1989; Mitchell, 1993; Haq and Davis, 1997; Haproff et al., 2018). Establishing the geologic history of the two flanking belts is crucial for understanding the holistic development of the Himalayan collisional system and differentiating the end-member models of continental deformation during the India-Asia collision (e.g., Tapponnier et al., 1982, 2001; England and Houseman, 1986; Cobbold and Davy, 1988; Dewey et al., 1988; England and Molnar, 1990; Royden et al., 1997; Zuza et al., 2019).

In this study, we investigate the divisions of major lithologic units exposed in the northern Indo-Burma Ranges, the northernmost segment of the Eastern

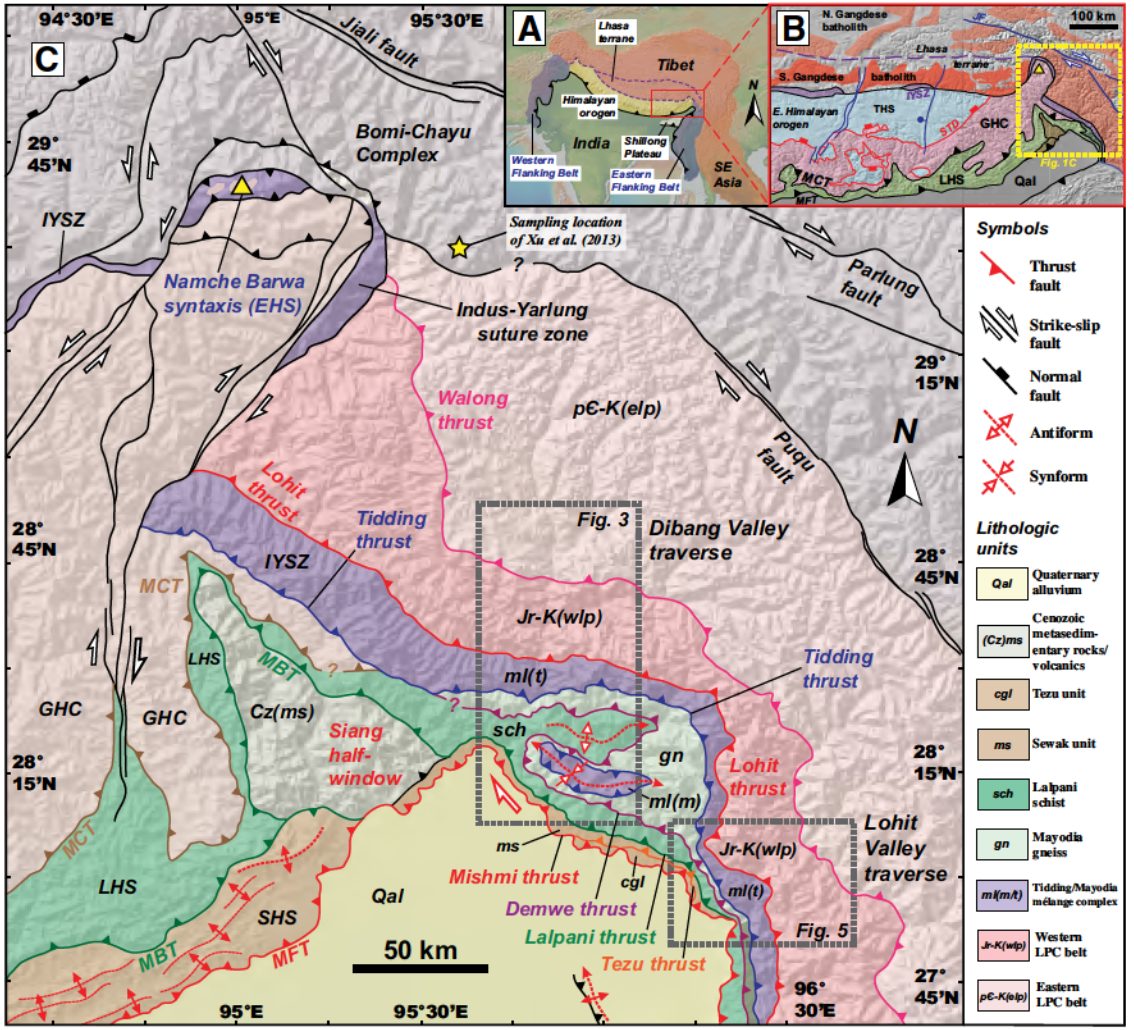

Figure 1. Geologic maps of (A) the Himalayan-Tibetan orogen; (B) the easternmost Himalayan orogen and southeastern Tibetan Plateau (modified from Webb et al., 2017); and (C) the northern Indo-Burma Ranges compiled from Ding et al. (2001) and Haproff et al. (2018). Abbreviations: EHS—eastern Himalayan syntaxis; GHC—Greater Himalayan Crystalline Complex; IYSZ—Indus-Yarlung suture zone; JF—Jiali fault; LHS—Lesser Himalayan Sequence; LPC—Lohit Plutonic Complex; MBT—Main Boundary thrust; MCT—Main Central thrust; MFT—Main Frontal thrust; STD—South Tibetan detachment; THS—Tethyan Himalayan Sequence.

Flanking Belt (Fig. 1). We correlate these units with the classic lithologic divisions of the Himalayan orogen and the Lhasa terrane to the west. Correlations are based on U-Pb zircon geochronology, whole-rock geochemistry, bounding Cenozoic faults, and similar lithologies. From these findings, we conclude that several lithologic units of the Himalayan-Tibetan orogen, including the Greater Himalayan Crystalline Complex, Tethyan Himalayan Sequence, Xigaze forearc basin, and Mesozoic–Cenozoic southern belt of the Gangdese batholith are absent in the study area. If these lithologic units were present at the onset of the India-Asia collision, our work implies a greater magnitude of crustal shortening and/or continental underthrusting across the northern Indo-Burma Ranges than across the Himalaya to the west.

GEOLOGIC SETTING

To provide a regional context, we summarize the existing research across the eastern Himalayan orogen, the Indus-Yarlung suture zone, the Lhasa terrane, cratonal rocks of northeast India, and the northernmost segment of the

Eastern Flanking Belt. The classic lithologic division of the Himalayan orogen includes from south to north: the Sub-Himalayan Sequence, Lesser Himalayan Sequence (LHS), Greater Himalayan Crystalline Complex (GHC), and Tethyan Himalayan Sequence (THS) (Yin, 2006) (Figs. 1B and 2). These Himalayan units are bounded to the north by the Indus-Yarlung suture zone, which has been shortened by two postcollisional thrust systems: the older south-directed Gangdese thrust system and the younger north-directed Great Counter thrust system (Yin et al., 1994, 1999; Harrison et al., 2000). Located north of the Indus-Yarlung suture zone, the Lhasa terrane exposes three east-trending tectonic belts from south to north: the Xigaze forearc basin and the southern and northern belts of the Gangdese batholith (Fig. 2).

Eastern Himalayan Orogen

The eastern Himalayan orogen referred to in this study extends from the Sikkim-Bhutan border at 89°E to the eastern Himalayan syntaxis at ~95°E (Figs. 1 and 2). The aforementioned major Himalayan lithologic units are tectonically juxtaposed by the following orogen-scale faults: the Main Frontal thrust at the base of the Sub-Himalayan Sequence, the Main Boundary thrust at the base of the LHS, the Main Central thrust at the base of the GHC, and the South Tibetan detachment at the base of the THS (e.g., Jangpangi, 1974; Acharyya and Ray, 1977; Gansser, 1983; Burchfiel et al., 1992; Acharyya, 1994; Bhargava, 1995; Edwards et al., 1996, 1999; Edwards and Harrison, 1997; Wu et al., 1998; Grujic et al., 2002; Yin et al., 2006, 2010a; McQuarrie et al., 2008; Long et al., 2011a, 2011b, 2011c; Burgess et al., 2012; Webb et al., 2013; DeCelles et al., 2016) (Fig. 2). Each of these faults is not expressed as a single structure but rather as a wide, km-scale zone of deformation comprising series of brittle faults and/or ductile shear zones (Hodges, 2000; Yin, 2006).

In the eastern Himalaya, the Sub-Himalayan Sequence consists of a ~4–6-km-thick section of Miocene–Pliocene sandstone and conglomerate (Gansser, 1983; Acharyya, 1994; Dikshitulu et al., 1995; Kumar, 1997; Yin et al., 2006; McQuarrie et al., 2008; Yin et al., 2010a) (Fig. 2). The LHS is composed of Neoproterozoic–Cambrian and Permian strata (Gansser, 1983; McQuarrie et al., 2008; Yin et al., 2010a; Long et al., 2011a) (Fig. 2). Various local names have been assigned for the LHS units in the eastern Himalaya, and their correlative relationships are illustrated in Figure 2. The base of the Proterozoic strata in the eastern Himalaya is marked by a meter-thick layer of quartz pebble conglomerate that was deposited atop a ca. 1.7 Ga augen gneiss (Yin et al., 2010a).

The GHC in the eastern Himalaya consists of metasediments, orthogneiss, metavolcanics, and Cenozoic leucogranites (e.g., Gansser, 1983; Yin et al., 2010a; Webb et al., 2013). In Bhutan, the north-dipping Kakhtang thrust, correlative to the Zimithang thrust to the east (Yin et al., 2006), divides the GHC into the upper and lower parts (Gansser, 1983; Swapp and Hollister, 1991; Grujic et al., 1996, 2002; Davidson et al., 1997; Daniel et al., 2003; McQuarrie et al., 2008; Long and McQuarrie, 2010; Yin et al., 2010a; Long et al., 2011a, 2011b) (Fig. 2). The upper GHC consists of upper amphibolite-facies orthogneiss, metasedimentary rocks, and Miocene leucogranites (Gansser, 1983; Swapp and Hollister, 1991; Grujic et al., 1996, 2002; Davidson et al., 1997; Daniel et al., 2003; Long et al., 2011b, 2011c; Zeiger et al., 2015). In the footwall of the Kakhtang thrust, the lower GHC consists of upper amphibolite-facies to upper greenschist-facies metasedimentary rocks and orthogneiss (Davidson et al., 1997; Daniel et al., 2003; Corrie et al., 2012; Zeiger et al., 2015). East of Bhutan, orthogneiss in the GHC yields U-Pb zircon age populations of ca. 1700 Ma, ca. 878 Ma, and ca. 500 Ma (Yin et al., 2010a) (Fig. 2), which are cut by ca. 20–18 Ma leucogranites (Aikman et al., 2012a, 2012b; Harrison and Wielicki, 2016). In the easternmost Himalaya along the Siang River Valley, the Main Central thrust splits into two thrusts referred to as the MCT-I and MCT-II by Nandini and Thakur (2011) (Fig. 2).

The THS above the South Tibetan detachment consists of pre-Triassic metasedimentary strata (Zeng et al., 2011) and Triassic–Cretaceous isoclinally folded marine strata (Yin et al., 1994, 1999; Harrison et al., 2000; Aikman et al., 2008) (Fig. 2). Folded THS strata are intruded by ca. 44 Ma granite (Aikman et al., 2008). Due to the merger of the Great Counter thrust and the South Tibetan detachment northwest of the eastern Himalayan syntaxis, the THS does not extend to the western margin of the eastern Himalayan syntaxis (Yin, 2006; Webb et al., 2013) (Figs. 1B and 2). The eastern Himalayan syntaxis is marked by the ~90° oroclinal bend in the general strike of thrust faults including the MFT, where the east-trending Himalayan orogen transitions to the north-trending northern Indo-Burma Ranges (Fig. 1).

Indus-Yarlung Suture Zone

The Indus-Yarlung suture zone consists of tectonic mélange complexes, dismembered ophiolitic sequences, subduction-related metamorphic rocks, syntectonic conglomerate deposits, and suprasubduction-related igneous rocks (Gansser, 1964; Honegger et al., 1982; Allégre et al., 1984; Malpas et al., 2003; Ziabrev et al., 2003; Dai et al., 2011a, 2011b; Hébert et al., 2012; Cai et al., 2012; An et al., 2014; Laskowski et al., 2016; Leary et al., 2016) (Fig. 1B). The suture zone involves Early Cretaceous ultramafic rocks, volcanics, volcaniclastic strata, granitoids, and carbonate, and fossiliferous chert and flysch are intermittently exposed along the northern margin of the Himalayan orogen (McDermid et al., 2002; Malpas et al., 2003; Ziabrev et al., 2003; Dubois-Côté et al., 2005; Dupuis et al., 2005; Zhou et al., 2005; Aitchison et al., 2007; Zhu et al., 2009b). These rocks are bounded by two Cenozoic thrust systems: the south-directed Gangdese thrust system of Harrison et al. (1992) and Yin et al. (1994) and the Great Counter thrust of the Heim and Gansser (1939).

Lhasa Terrane

The Lhasa terrane is a ~200–300-km-wide continental strip that trends east-west in southern Tibet and wraps around the eastern Himalayan

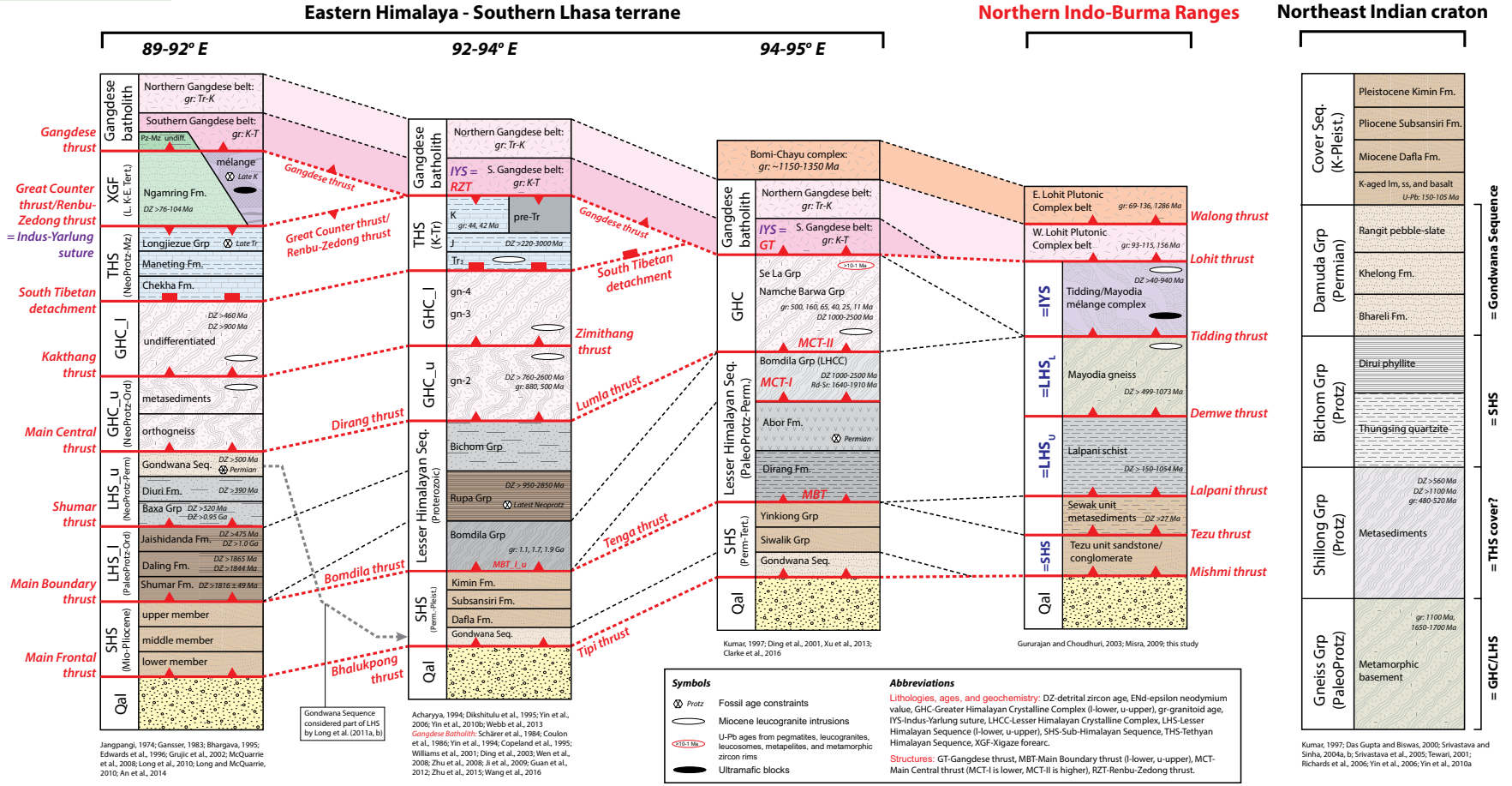

Figure 2. Tectonostratigraphic sections of the eastern Himalaya, the Lhasa terrane, the northern Indo-Burma Ranges, and the northeast Indian craton. Possible correlations between lithologic units are shown.

syntaxis to a north-south trend in northern Myanmar and western Yunnan of China (e.g., Lin et al., 2013; Wang et al., 2014) (Fig. 1B). The terrane is divided into northern and southern halves by an east-trending ophiolite belt, which was interpreted to be a suture zone or a zone of rootless klippe sourced from the Bangong-Nujiang suture zone in the north (Girardeau et al., 1984; Coward et al., 1988; Hsü et al., 1995; Yin and Harrison, 2000; Kapp et al., 2003; Dong et al., 2011, Zhu et al., 2012; Zhang et al., 2014). The Lhasa terrane exposes Mesoproterozoic orthogneiss in the easternmost Bomi-Chayu Complex (ca. 1250–1350 Ma) (Xu et al., 2013), a composite Neoproterozoic (ca. 920–820 Ma) and Cambro-Ordovician (ca. 540–460 Ma) gneiss complex along the northern margin of the Lhasa terrane (Guynn et al., 2012), and fragments of Devonian orthogneiss (ca. 366 Ma) in southeast Tibet (Zhu et al., 2011) (Figs. 1 and 2).

The salient feature of the Lhasa terrane is the >2000-km-long Mesozoic to earliest Cenozoic Gangdese batholith belt of Chang and Zheng (1973) (Fig. 1B). The batholith belt can be divided into the northern and southern belts: the northern belt is characterized by Late Triassic plutons (Wang et al., 2016), Cretaceous adakite (Zhu et al., 2009a), and S-type granitoids (Wen et al., 2008), whereas the southern belt is dominated by Cretaceous to Eocene granitoids overlain by Paleocene–Eocene volcanic strata (Schärer et al., 1984; Coulon et

al., 1986; Copeland et al., 1995; Ding et al., 2003; Wen et al., 2008; Zhu et al., 2008; Ji et al., 2009; Lee et al., 2009; Guan et al., 2012).

The southern part of the Lhasa terrane is marked by the Gangdese thrust system, which juxtaposes strata of the Xigaze forearc basin strata and the Gangdese batholith over the THS (Fig. 2) (Yin et al., 1994). The Xigaze forearc basin sequence consists of Cretaceous to Eocene marine deposits on top of an oceanic basement (Garzanti and Van Haver, 1988; Einsele et al., 1994; Dürr, 1996; Ding et al., 2005; Wang et al., 2012; An et al., 2014; Hu et al., 2015; Orme et al., 2015). The forearc strata are only exposed in south-central Tibet and are absent in southwest and southeast Tibet along strike. This map pattern is interpreted to be a result of postcollisional underthrusting of the Xigaze forearc basin below the Gangdese batholith (Yin et al., 1994, 1999; Harrison et al., 2000). The Cretaceous strata are intruded by a series of north-trending dikes that yield ages of ca. 18–14 Ma (Yin et al., 1994; Williams et al., 2001).

Cratonal Rocks of Northeast India

The 400-km-long, east-trending Shillong Plateau of northeast India exposes Indian cratonal rocks that are correlative to the Proterozoic metasedimentary strata and Precambrian crystalline rocks of the LHS and GHC (e.g., Gansser, 1983; Gupta and Biswas, 2000; Srivastava and Sinha, 2004a, 2004b; Srivastava et al., 2005; Richards et al., 2006; Tewari et al., 2010; Yin et al., 2010b) (Fig. 1A). Cenozoic deformation is expressed by east-striking thrust faults that bound the margins of the plateau (e.g., Clark and Bilham, 2008; Yin et al., 2010b). Active deformation within the Shillong Plateau is evident by multiple northeast-striking left-slip faults that offset Quaternary geomorphic features and sediments (Yin et al., 2010b).

Northern Indo-Burma Ranges

The research presented here is focused on the northern Indo-Burma Ranges, the northernmost segment of the Eastern Flanking Belt, which is located north of latitude 27°N (Fig. 1). Previous geological studies have established the first-order lithologic framework of the northern Indo-Burma Ranges (e.g., Wadia, 1931; Nandy, 1973; Thakur and Jain, 1975; Acharyya, 1980, 1987; Sharma et al., 1991; Singh, 1993; Misra and Singh, 2002; Gururajan and Choudhuri, 2003; Goswami, 2008, 2011; Misra, 2009; Sarma et al., 2009; Sarma et al., 2012; Goswami, 2013a, 2013b; Sharma and Sarma, 2013; Ningthoujam et al., 2015). Most recently, Haproff et al. (2018) divided the exposed rocks into six lithologic units (Figs. 3–5), which from northeast to southwest consist of: (1) igneous rocks of the Lohit Plutonic Complex (Fig. 6); (2) the Tidding mélange complex (Fig. 7); (3) metamorphic rocks of the Mayodia gneiss (Fig. 8); (4) metasedimentary rocks of the Lalpani schist (Fig. 9); (5) siliciclastic strata of the Tezu unit (Fig. 10A); and (6) metasedimentary rocks of the Sewak unit (Fig. 10B). In this paper, we further subdivide the exposures of mélange rocks into the Tidding and Mayodia mélange complexes based on their map-view separation (Fig. 3). Each lithologic unit is bounded by south- to west-directed thrust faults including (1) the Walong thrust, (2) the Lohit thrust, (3) the Tidding thrust, (4) the Demwe thrust, (5) the Lalpani thrust, (6) the Tezu thrust, and (7) the Mishmi thrust (Fig. 2). Despite extensive work in the northern Indo-Burma Ranges, disagreement remains whether these lithologic units are correlative with those of the Himalayan orogen and the Lhasa terrane (e.g., Thakur and Jain, 1975; Acharyya, 1980; Singh and Chowdhury, 1990; Gururajan and Choudhuri, 2003; Misra, 2009). Furthermore, previous lithologic correlations are solely based on comparable lithologies and remain untested with geochronologic or geochemical techniques (e.g., Gururajan and Choudhuri, 2003; Misra, 2009).

This study builds upon the work of Haproff et al. (2018), which described the structural framework of the northern Indo-Burma Ranges with a focus on the kinematics of major faults. Here we focus on the lithologies, geochemical compositions, and geochronologic ages of the thrust-bounded lithologic units and investigate how they correlate with those of the Himalayan orogen and the Lhasa terrane to the west (Fig. 2). Such an approach provides additional constraints on the possible evolutionary history of the Himalayan collisional system including both the Himalayan orogen and Eastern and Western Flanking Belts.

SAMPLING AND ANALYTICAL METHODS

A total of 65 samples were collected along the Lohit and Dibang Valleys for U-Pb zircon geochronology and whole-rock geochemistry (Figs. 3–5). Sampling locations and detailed methodologies are described below. We also present additional geologic maps of Dibang Valley (Fig. 4) and more detailed descriptions of lithologic units.

U-Pb Zircon Geochronology of the Lohit Plutonic Complex

Zircon grains from ten samples of the Lohit Plutonic Complex were analyzed for U-Pb crystallization ages using secondary ion mass spectrometry (SIMS) (Cameca ims-1270 ion microprobe) at University of California, Los Angeles (UCLA) (Table 1). Prior to analysis, zircon grains were mounted with standard AS3 (1099 Ma; Paces and Miller, 1993) on 1-inch-diameter epoxy mounts, polished with carbide paper, and coated with ~100 Å of gold. Cathodoluminescence (CL) images were taken using the scanning electron microscope (SEM) at UCLA to observe any zonation. Zircons were sputtered using a 10–15 nA O^- primary beam on ~25-µm-diameter spots on zircon rims. U-Pb isotopic ratios ($^{206}Pb/^{238}U$ and $^{207}Pb/^{235}U$) were calculated based on a calibration curve of UO/U versus Pb/U, and corrected for common lead (Stacey and Kramers, 1975). $^{207}Pb/^{206}Pb$ ages were reported for zircon grains of >1000 Ma age. Data reduction was accomplished using the program ZIPS 3.0.3, and weighted-mean ages, concordia diagrams, and relative probability plots were

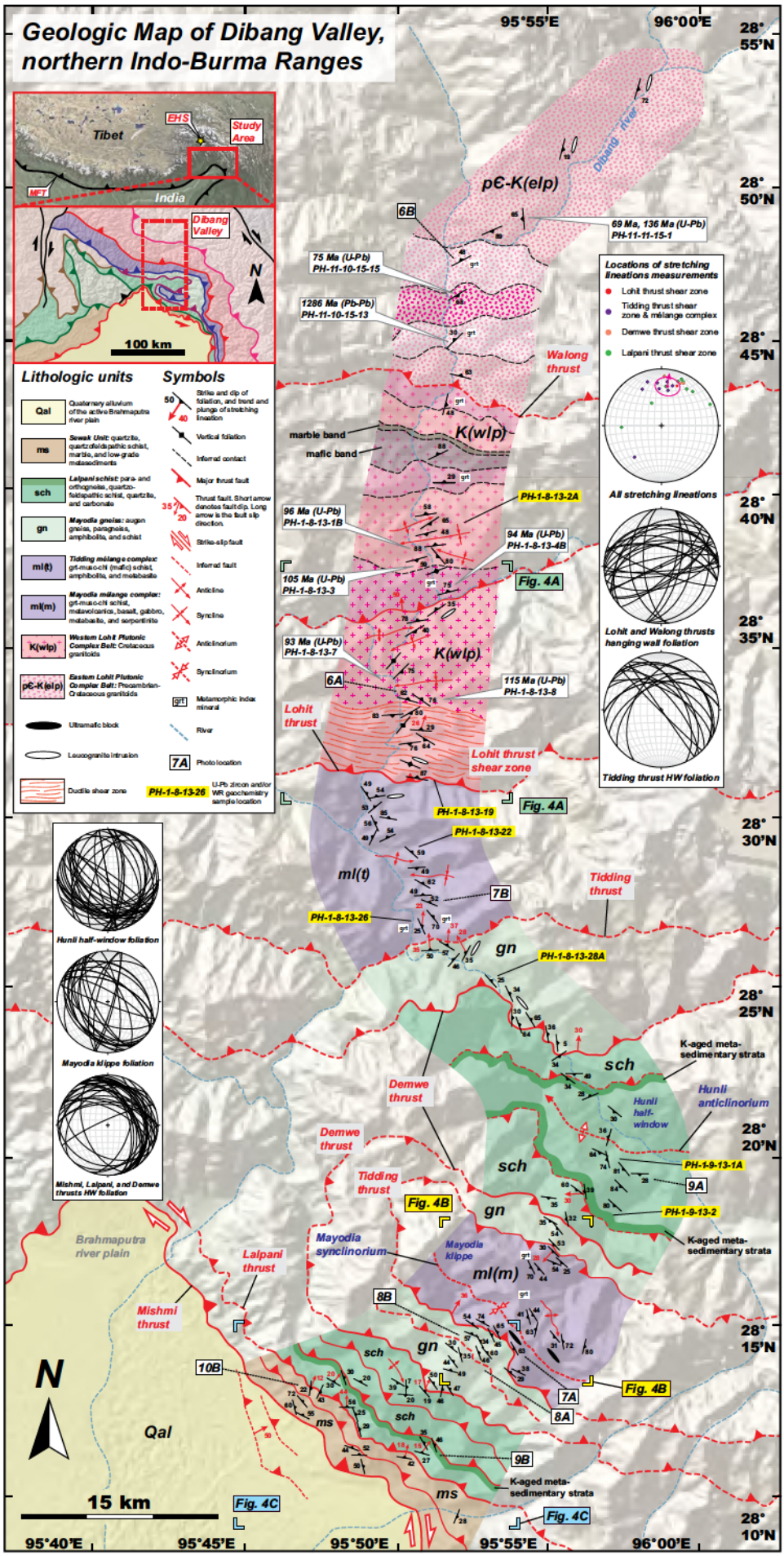

Figure 3. Geologic map of Dibang Valley modified from Haproff et al. (2018). See Figure 4 for additional sample locations. Abbreviations: EHS—eastern Himalayan syntaxis; HW—hanging wall; MFT—Main Frontal thrust; and WR—whole-rock.

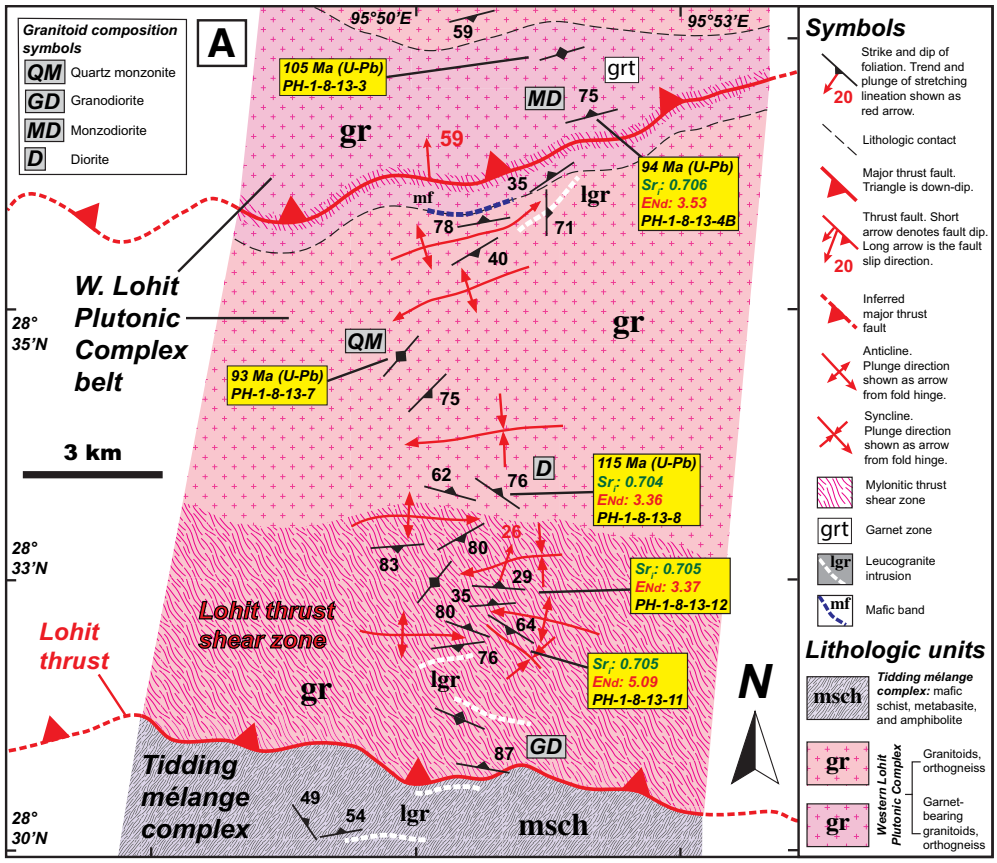

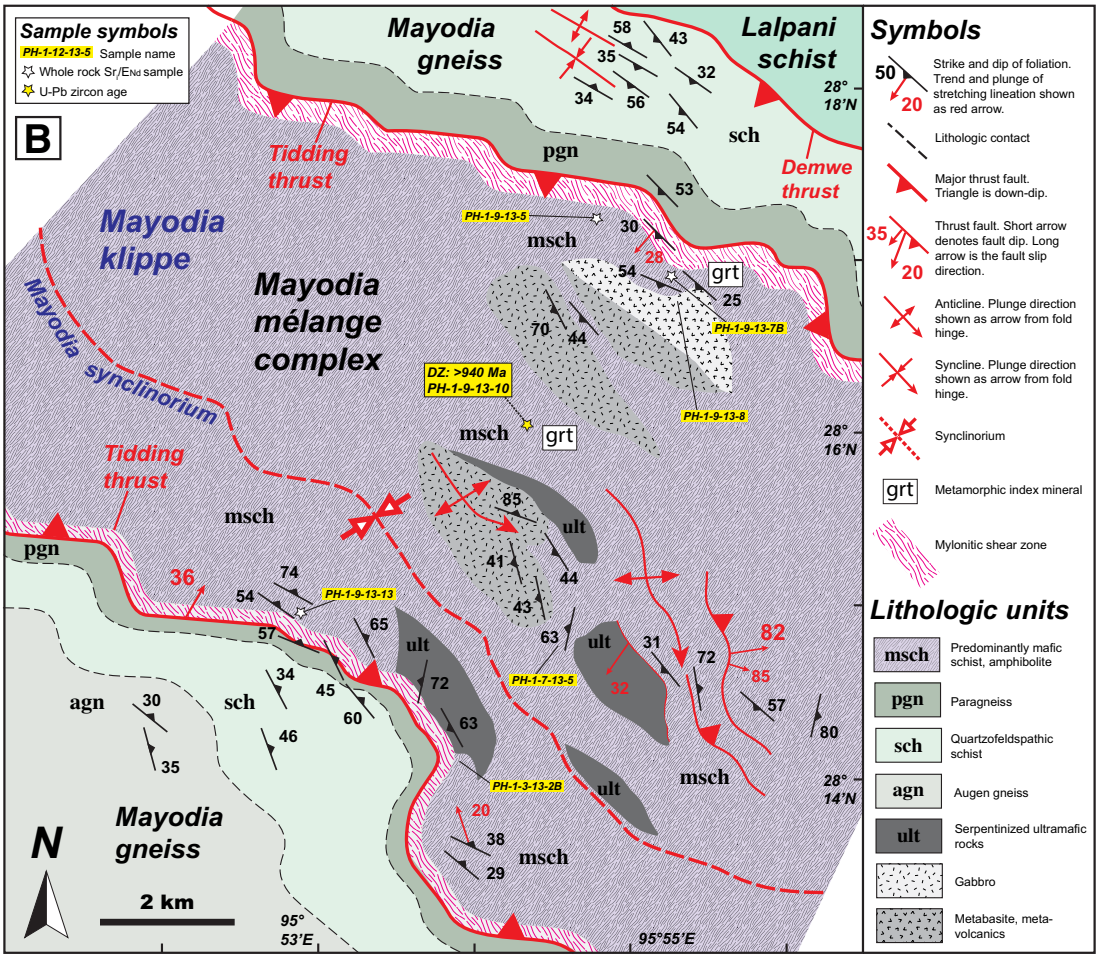

Figure 4. Detailed geologic maps of (A) the foreland region; (B) Mayodia klippe; and (C) Lohit thrust shear zone along the Dibang Valley traverse. The locations of samples for whole-rock geochemistry and U-Pb zircon geochronology are shown. Abbreviations: DZ—detrital zircon. (*Continued on following page.*)

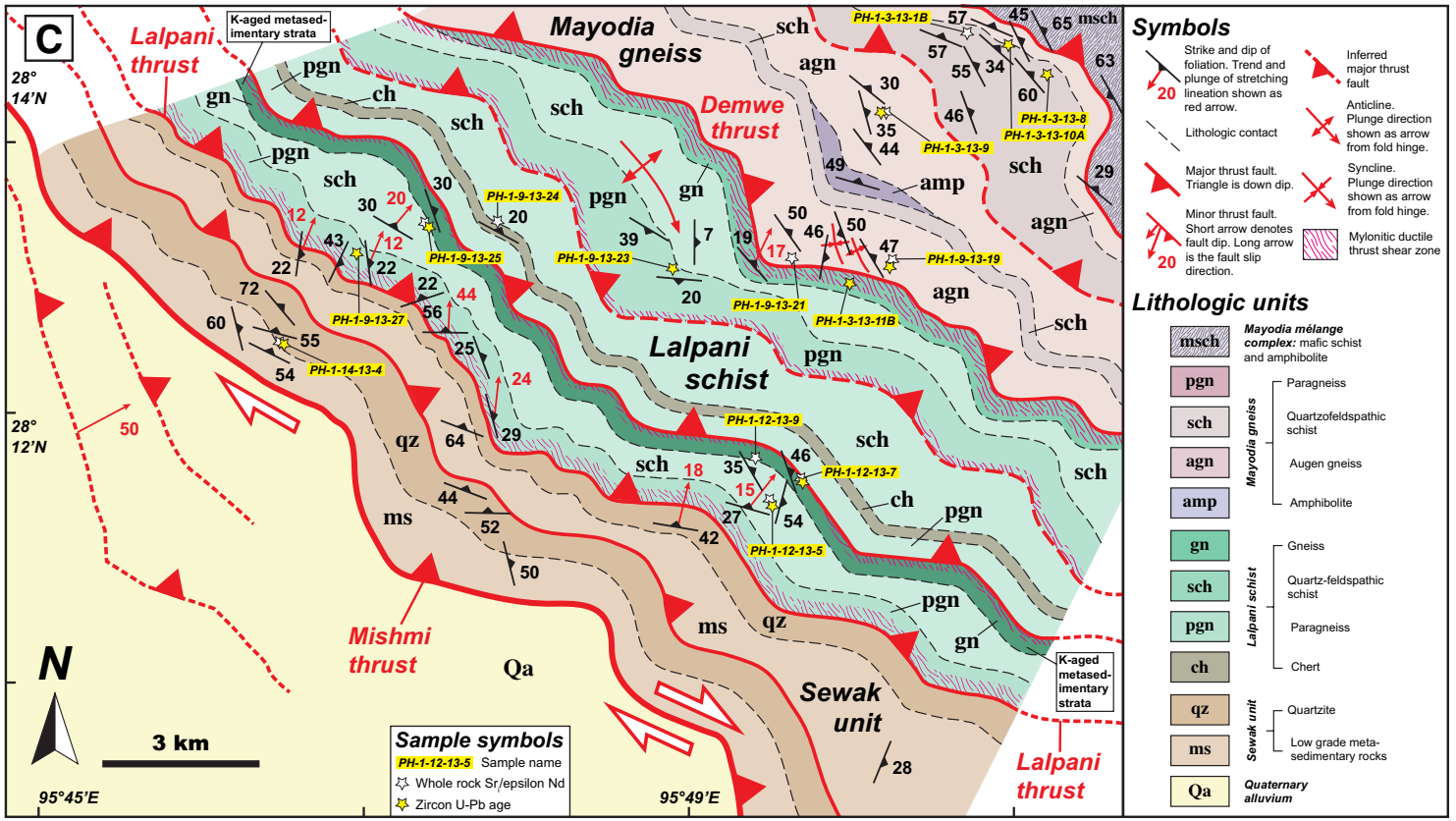

Figure 4 (*continued*).

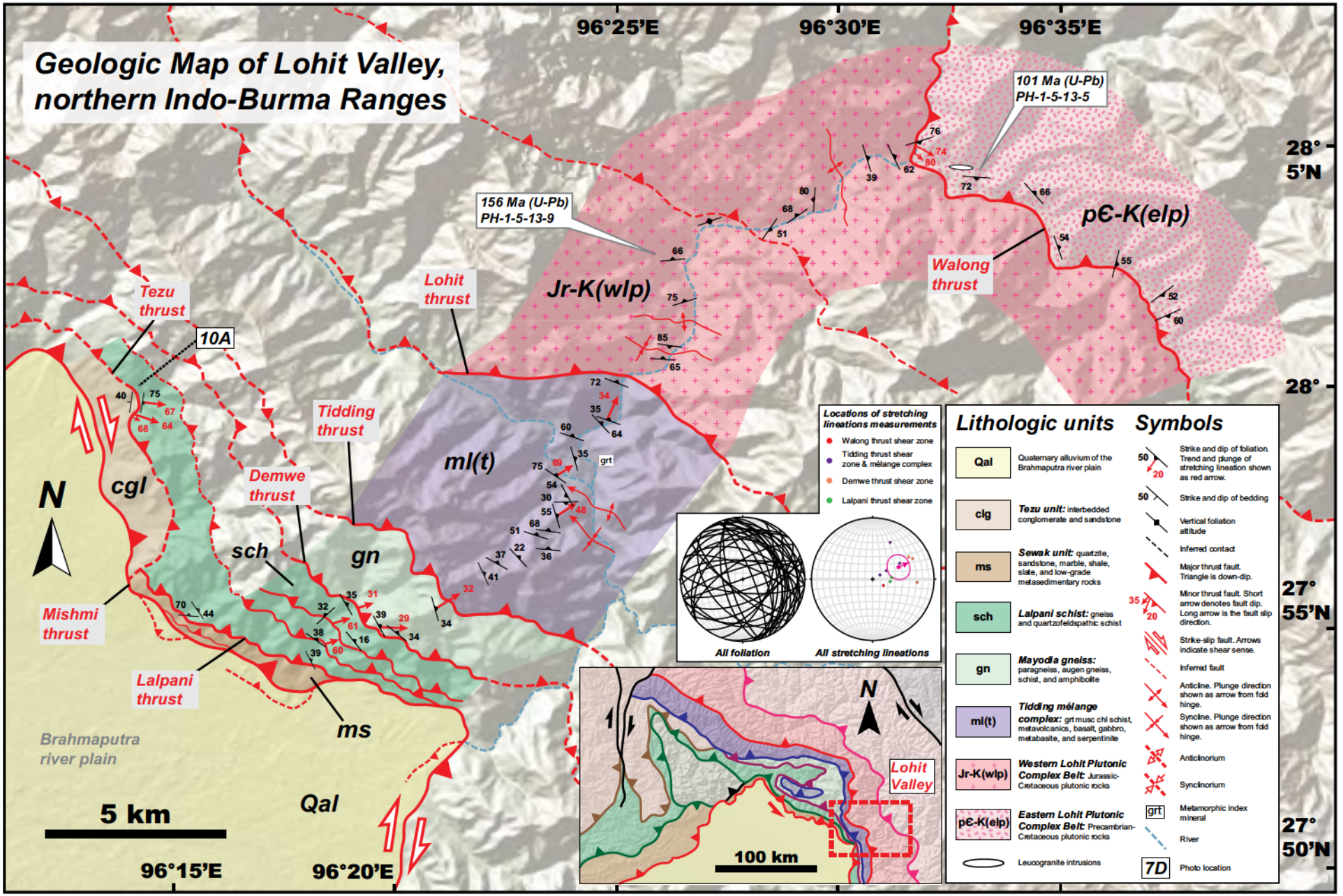

Figure 5. Geologic map of Lohit Valley modified from Haproff et al. (2018).

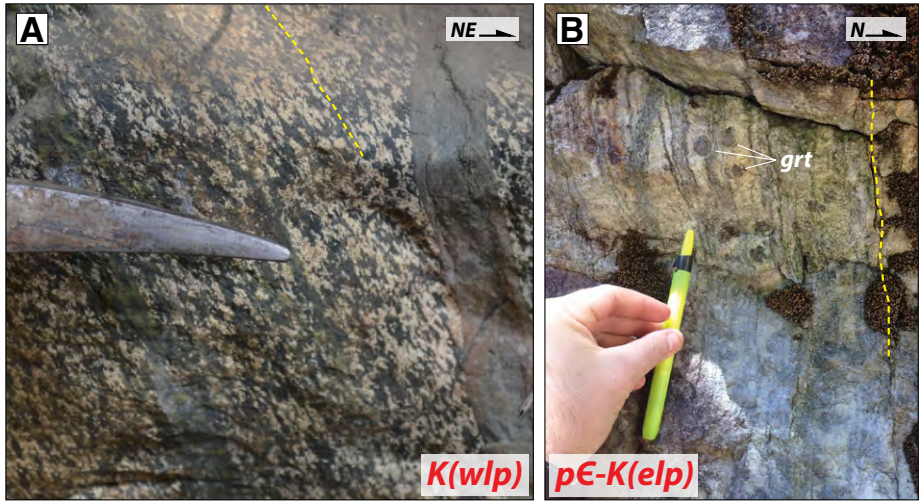

Figure 6. Outcrop photographs of the Lohit Plutonic Complex (LPC) including (A) foliated diorite of the western LPC belt and (B) garnet-bearing orthogneiss of the eastern LPC belt. The yellow dashed lines depict the orientation of foliation.

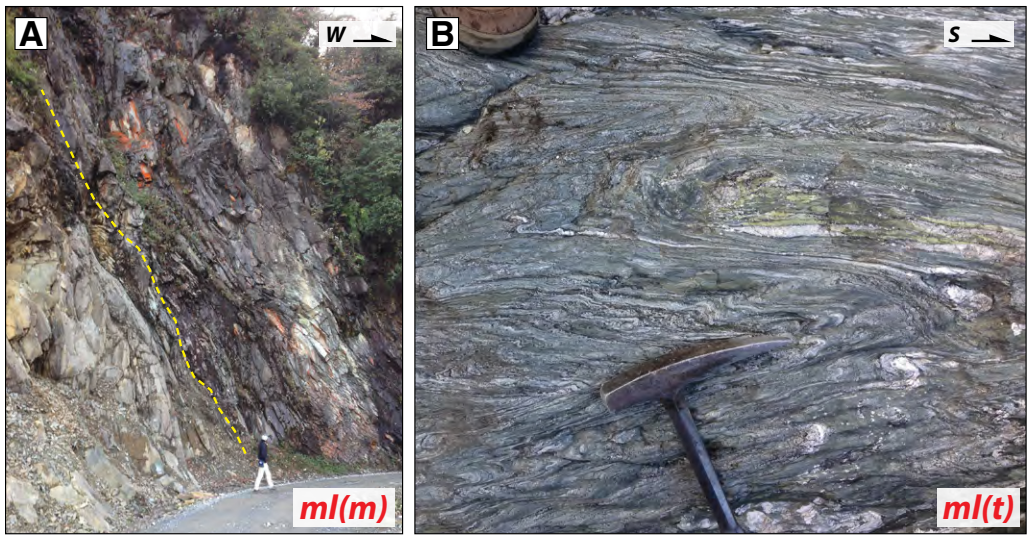

Figure 7. Outcrop photographs of (A) sheared serpentinite in the Mayodia mélange complex and (B) isoclinally folded chlorite schist in the Tidding mélange complex. The yellow dashed line depicts the orientation of foliation.

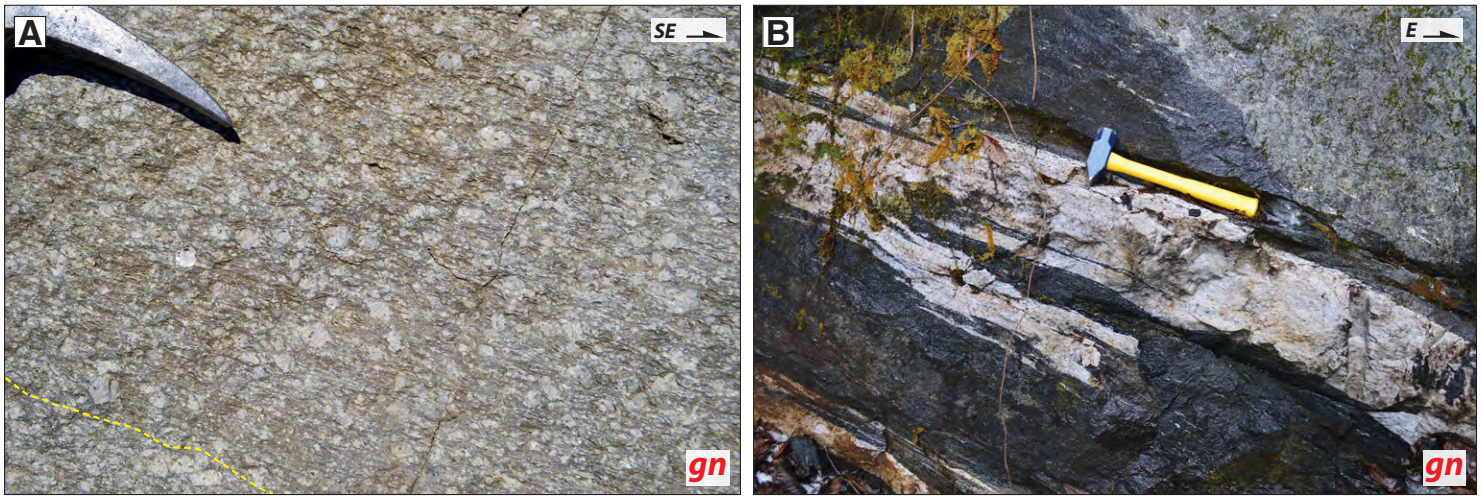

Figure 8. Outcrop photographs of the Mayodia gneiss in Dibang Valley including (A) augen gneiss and (B) gneiss intruded by a meter-scale leucogranite vein. The yellow dashed line depicts the orientation of foliation.

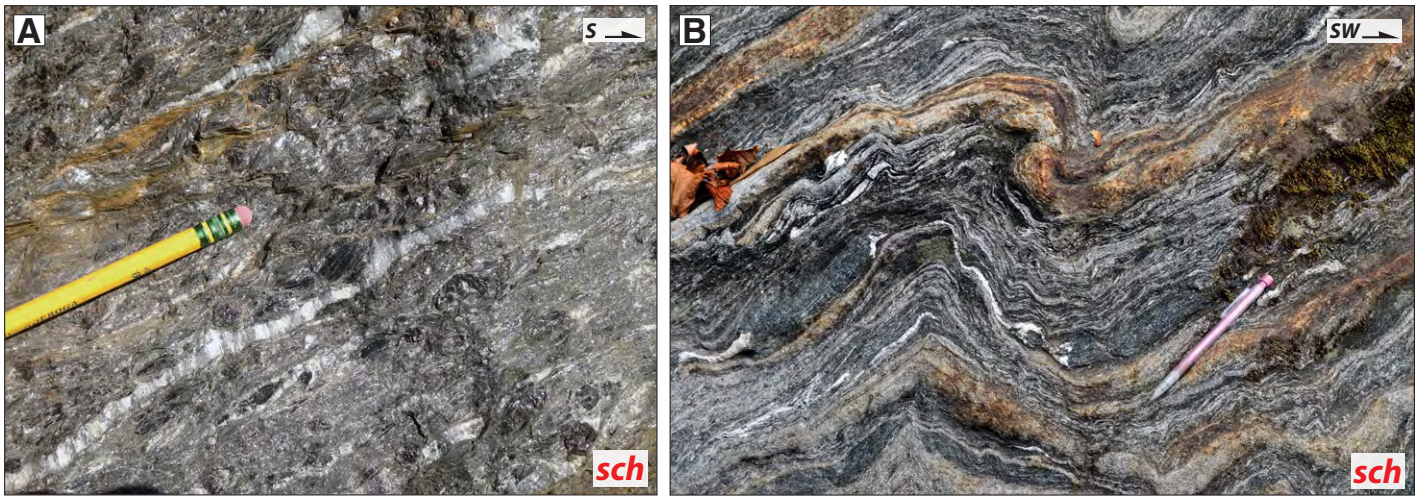

Figure 9. Outcrop photographs of the Lalpani schist including (A) mica schist and (B) southwest-verging isoclinal folds within paragneiss (Haproff et al., 2018).

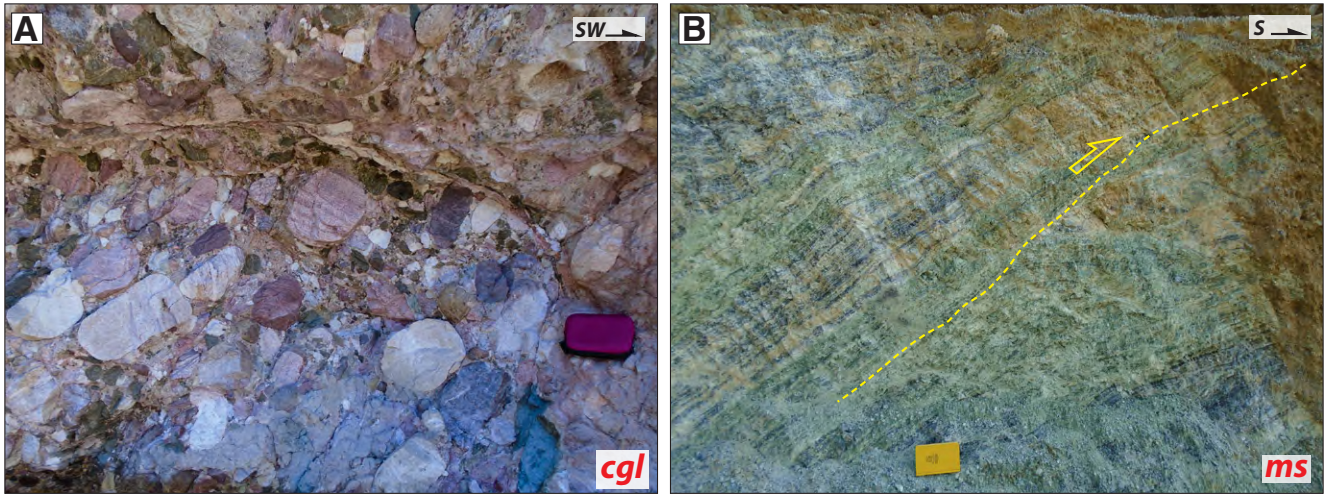

Figure 10. Outcrop photographs of (A) conglomerate in the Tezu unit and (B) a meter-scale, south-directed thrust within a quartzite unit of the Sewak unit.

TABLE 1. SUMMARY OF ZIRCON U-Pb GEOCHRONOLOGY RESULTS OF THE LOHIT PLUTONIC COMPLEX

Sample	Rock type	Latitude	Longitude	Elevation (m)	Age (Ma) (±2σ)	MSWD	n
Western Lohit Plutonic Complex Belt							
PH-1-8-13-1B	Monzodiorite	N28° 37.975	E95° 51.138	798	96.3 ± 3	1.5	13 out of 18
PH-1-8-13-3	Tonalite	N28° 37.309	E95° 51.362	734	105.4 ± 3	1.2	11 out of 11
PH-1-8-13-4B	Monzodiorite	N28° 36.754	E95° 51.718	717	94 ± 20	3.3	3 out of 3
PH-1-8-13-7	Quartz monzonite	N28° 34.809	E95° 50.009	688	93.7 ± 3	0.2	10 out of 10
PH-1-8-13-8	Diorite	N28° 33.579	E95° 50.865	736	115 ± 13	3.5	8 out of 10
PH-1-5-13-9	Diorite	N28° 33.170	E95° 50.510	783	156.7 ± 7	1.5	8 out of 8
Eastern Lohit Plutonic Complex Belt							
PH-11-10-15-15	Orthogneiss	N28° 45.925	E95° 52.060	1286	75.6 ± 9	7.7	15 out of 17
PH-11-11-15-1 (A)[1]	Orthogneiss	N28° 47.281	E95° 54.543	1357	136.2 ± 5	0.89	22 out of 26
PH-11-11-15-1 (B)	Orthogneiss	N28° 47.281	E95° 54.543	1357	69.3 ± 9	0.1	2 out of 26
PH-11-10-15-13[2]	Orthogneiss	N28° 43.646	E95° 51.839	1080	1286 ± 14	5.7	9 out of 14
PH-1-5-13-5	Diorite	N28° 4.258	E96° 33.112	623	101.2 ± 5	0.3	10 out of 10

[1]Sample PH-11-11-15-1 yielded a bimodal age distribution of mid-Cretaceous (A) and Late Cretaceous (B) zircons.
[2]Weighted-mean age is determined from the single main population of Mesoproterozoic ^{207}Pb-^{206}Pb ages. MSWD—mean square of weighted deviates.

generated using Isoplot/Ex (Ludwig, 1991). Data tables of all zircon analyses are shown in Tables S1 and S2 in the Supplemental Materials[1]. Analyses were excluded for low radiogenic lead concentrations, large analytical errors, inherited zircon grains that were significantly older than the dominant zircon-age population, and discordant ages. We calculated the weighted-mean age of the youngest population of concordant analyses to estimate the crystallization age of the plutonic samples.

U-Pb Detrital Zircon Geochronology

Detrital zircons from 15 metasedimentary rocks from the Sewak unit, Lalpani schist, Mayodia gneiss, and Tidding and Mayodia mélange complexes were dated via U-Pb geochronology (Table 2). Complete isotopic data of all detrital zircon analyses are shown in Tables S3–S6 (see footnote 1). Zircon age distributions were used to determine the detrital provenance, distinguish lithologic units, and test correlations with metasedimentary rocks of the Himalayan orogen to the west of the study area.

Zircon grains were separated from rocks at UCLA using standard procedures (Quidelleur et al., 1997; Schmitt et al., 2003a, 2003b). Zircons were mounted on 1-inch-diameter epoxy rounds with 91500 zircon standards (1065 Ma age; Wiedenbeck et al., 1995) and were polished with carbide paper. Zircons from two samples were analyzed by laser ablation–inductively coupled plasma mass spectrometry (LA-ICP MS) at the University of California, Santa Barbara (see Kylander-Clark et al., 2013 for detailed analytical methods). Spot sizes of ~20 μm were each shot twice with an excimer laser at a 5 Hz pulse rate. Zircon grains from another 13 samples were analyzed using the method of Liu et al. (2018) at the Institute of Tibetan Plateau Research, Chinese Academy of Sciences in Beijing, China.

TABLE 2. LIST OF SAMPLES USED FOR DETRITAL ZIRCON U-Pb GEOCHRONOLOGY

Sample	Rock type	Latitude	Longitude	Elevation (m)	Youngest age (Ma) (±2σ)
Sewak unit					
PH-1-14-13-4	Phyllite	N28° 12.686	E95° 46.841	417	27 ± 1
Lalpani schist					
PH-1-9-13-2	Schist	N28° 18.625	E95° 57.287	1196	150 ± 4
PH-1-12-13-7	Paragneiss	N28° 11.524	E95° 51.062	571	158 ± 1
PH-1-9-13-25	Paragneiss	N28° 13.478	E95° 48.126	1170	177 ± 1
PH-1-3-13-11B	Paragneiss	N28° 13.167	E95° 51.687	1810	525 ± 3
PH-1-9-13-23	Schist	N28° 13.098	E95° 50.312	1483	1054 ± 19
PH-1-12-13-5	Paragneiss	N28° 11.415	E95° 50.882	542	913 ± 5
PH-1-9-13-27	Paragneiss	N28° 13.131	E95° 47.572	1064	974 ± 6
Mayodia gneiss					
PH-1-3-13-9	Paragneiss	28° 14.484	E95° 53.241	2062	499 ± 3
PH-1-3-13-10A	Schist	N28° 14.304	E95° 51.994	1811	646 ± 13
PH-1-3-13-8	Paragneiss	N28° 14.745	E95° 53.110'E	2061	1069 ± 13
PH-1-9-13-19A	Paragneiss	N28° 13.263	E95° 51.781	1639	1022 ± 16
PH-1-9-13-19B	Paragneiss	N28° 13.307	E95° 51.783	1645	1073 ± 19
Tidding and Mayodia mélange complexes					
PH-1-8-13-26	Schist	N28° 26.897	E95° 50.957	729	40 ± 1
PH-1-9-13-10	Schist	N28° 16.145	E95° 54.358	2363	940 ± 9

Whole-Rock Geochemistry

Whole-rock major- and trace-element geochemical analyses were conducted on six plutonic samples from the Lohit Plutonic Complex and nine mafic and ultramafic samples. Samples selected for whole-rock geochemical analyses were crushed using a steel mortar and pestle and were pulverized. Major-, minor-, and trace-element compositions were determined by LA-ICP MS at Activation Laboratories (Actlabs) in Ontario, Canada. Major- and minor-element compositions of nine whole-rock samples were determined at Pomona College by fusion of Li tetraborate and X-ray fluorescence (XRF) analysis using a PanAnalytical Axios wavelength-dispersive instrument. XRF instrument calibration and sample preparation methods are based on Johnson et al. (1999). Trace-element compositions were determined via ICP-MS at the Institute of Tibetan Plateau Research, Chinese Academy of Sciences in Beijing using the methods of Liu et al. (2018). Results of major- and trace-element geochemistry are shown on Tables S7 and S8 (see footnote 1). Four samples of the western Lohit Plutonic Complex belt were cut into thin sections and viewed with a petrographic microscope to determine the modal abundances of quartz, plagioclase, and alkali feldspar for granitoid classification (Fig. S4B [see footnote 1]).

Twenty-one plutonic and metasedimentary rock samples from each major lithologic unit were analyzed for $^{143}Nd/^{144}Nd$ and/or initial $^{87}Sr/^{86}Sr$ (Sr_i) isotopic ratios to understand the source and setting of magma genesis and to test correlation with rocks of the Himalayan orogen (Table 3). Prior to analysis, powdered samples were first placed in Teflon bombs, diluted with H_2O, HNO_3, and HF, and oven heated at 190 °C for 36 h. Four ml of H_2O, $HClO_4$, and HNO_3 were added to solution, along with 0.1 ml Rh and Re internal standard. Final sample preparation and analyses were performed using the methods of Liu et al. (2018) via both LA-ICP-MS and thermal ionization mass spectrometry (TIMS) at the Institute of Tibetan Plateau Research in Beijing and Guangzhou, China.

LITHOLOGIC UNITS OF THE NORTHERN INDO-BURMA RANGES AND RESULTS OF U-Pb ZIRCON GEOCHRONOLOGY

Lohit Plutonic Complex

The northernmost mapped unit is the Lohit Plutonic Complex of Nandy (1973), which is divided into western and eastern belts by the north-dipping

SUPPLEMENTARY MATERIALS

Figure Captions

Figure S1. U-Pb zircon concordia, relative probability, and weighted mean age plots for granitoids of the western Lohit Plutonic Complex belt: (A) *PH-1-8-13-1B*, (B) *PH-1-8-13-3*, (C) *PH-1-8-13-4B*, (D) *PH-1-8-13-7*, (E) *PH-1-8-13-8*, and (F) *PH-1-5-13-9*.

Figure S2. U-Pb concordia, relative probability, and weighted mean age plots for granitoids of the eastern Lohit Plutonic Complex belt: (A) *PH-11-10-15-15*, (B) *PH-11-11-15-1*, (C) *PH-11-10-15-13*, and (D) *PH-1-5-13-5*.

Figure S3. Cathodoluminescence images of representative zircons analyzed for U-Pb crystallization ages from (A-C) granitoids of the western Lohit Plutonic Complex belt and (D) diorite of the eastern Lohit Plutonic Complex belt.

Figure S4. Geochemical plots for plutonic rocks including (A) K_2O vs. SiO_2 (Le Bas et al., 1984) and (B) granitoid-type based on quartz-alkali feldspar-plagioclase feldspar (QAP) abundances based on mineral point counting in thin section.

Figure S5. Diagrams of sources for plutonic rocks including anorogenic (*A*), igneous (*I*), sedimentary (*S*), and mantle (*M*) -types based on (A) $K_2O + N_2O$ vs. 10000*Ga/Al and (B) Nb vs. 10000*Ga/Al. Tectonic settings diagram for plutonic rocks including syncollisonal (*syn-COLG*), within-plate granite (*WPG*), volcanic arc granite (*VAG*), orogenic (*ORG*) based on (C) Ta vs. Yb and (D) Rb vs. Y + Nb (Pearce et al., 1984).

1

[1]Supplemental Materials. U-Pb zircon concordia diagrams and tabulated data, zircon cathodoluminescence images, and geochemical plots and tabulated data. Please visit https://doi.org/10.1130/GES02054.S1 or access the full-text article on www.gsapubs.org to view the Supplemental Materials.

TABLE 3. SUMMARY OF WHOLE-ROCK Nd AND SR ISOTOPIC DATA

Sample	Rock type	Rb (ppm)	Sr (ppm)	Sm (ppm)	Nd (ppm)	$^{87}Sr/^{86}Sr$	2 S.E.	$^{143}Nd/^{144}Nd$	2 S.E.	ε_{Nd}[1]
Eastern Lohit Plutonic Complex										
PH-11-10-15-13	Migmatitic orthogneiss	3	197	5.7	18.1	0.7051	2.0E-5	-	-	-
Western Lohit Plutonic Complex										
PH-1-8-13-1B	Monzodiorite	101	814	3.6	15.3	0.7053	3.2E-05	0.5127	9.0E-06	2.22
PH-1-8-13-4B	Monzodiorite	113	368	4.1	18.3	0.7055	3.0E-05	0.5128	7.0E-06	3.53
PH-1-8-13-8	Diorite	34	738	2.2	11.1	0.7042	2.0E-05	0.5128	9.0E-06	3.36
PH-1-8-13-11	Mafic dike	7	188	2.7	9.4	0.7052	2.0E-05	0.5129	1.0E-05	5.09
PH-1-8-13-12A	Granodiorite	3.1	205	1	4.7	0.7045	2.8E-05	0.5128	1.4E-05	3.37
Tidding and Mayodia mélange complexes										
PH-1-9-13-7B	Ultramafic rock	22	310	4.8	18.7	0.7053	2.2E-05	0.5130	7.0E-06	7.69
PH-1-8-13-22	Granitoid intrusion	35.3	483.7	2.7	20.9	0.7055	1.8E-05	0.5127	8.0E-06	0.84
PH-1-8-13-26	Garnet schist	70.7	311.3	8.4	42.2	0.7124	1.8E-05	0.5123	5.0E-06	–7.22
PH-1-9-13-13	Metabasalt	3	180	3.5	10.2	0.7061	2.7E-05	0.5129	1.7E-05	5.41
PH-1-9-13-5	Mica schist	60	627	8.9	45	0.7043	2.8E-05	0.5129	2.1E-05	4.97
Mayodia gneiss										
PH-1-9-13-19B	Paragneiss	267	75	9.4	47.2	0.9116	2.2E-05	0.5117	8.0E-06	–17.48
PH-1-9-13-19A	Paragneiss	303	58	8	35.7	-	-	0.5118	6.0E-06	–15.47
PH-1-3-13-1B	Biotite schist	39.3	251.6	1.6	29.2	0.7209	2.2E-05	0.5118	8.0E-06	–16.39
PH-1-3-13-9	Augen gneiss	73	248.5	2	41.6	0.7153	1.6E-05	0.5121	8.0E-06	–10.34
Lalpani schist										
PH-1-9-13-1A	Mica schist	124.8	216.8	4	19.7	0.7085	1.8E-05	0.5124	9.0E-06	–5.46
PH-1-12-13-9	Paragneiss	194	64	11.6	70.6	0.7569	2.4E-05	0.5117	7.0E-06	–19.74
PH-1-9-13-25	Paragneiss	298.5	11.2	0.4	46	0.8945	3.2E-05	0.5117	6.0E-06	–18.08
PH-1-12-13-5	Paragneiss	176	136	8.9	51.3	0.7441	2.2E-05	0.5112	6.0E-06	–27.76
PH-1-9-13-24	Quartzite	32	8	9.7	29.9	0.7812	2.2E-05	0.5118	9.0E-06	–15.96
Sewak unit										
PH-1-14-13-4	Phyllite	55	150	4.6	22.9	0.7117	1.8E-05	0.5121	6.0E-06	–10.16

[1]Epsilon notation (ε_{Nd}) is determined by normalizing sample $^{143}Nd/^{144}Nd$ values to the chondritic uniform reservoir (CHUR).

Walong thrust (Gururajan and Choudhuri, 2003) (Figs. 3, 4A, and 5). Ten samples were collected from the eastern and western belts to constrain the spatial distribution of U-Pb zircon ages.

Western Lohit Plutonic Complex Belt

The western belt of the Lohit Plutonic Complex consists of diorite, granodiorite, monzodiorite, tonalite, quartz monzonite (Fig. 6A), and younger leucogranite and mafic dikes thrust over the Tidding mélange complex (Fig. 4A). The locations of six samples collected for U-Pb zircon geochronology are shown on Figs. 3, 4A, and 5. Samples contain quartz, plagioclase, potassium feldspar, biotite, and variable hornblende and garnet. Some samples also contain epidote, clinozoisite, rutile, ilmenite, and zoned garnet. Cathodoluminescence images of representative zircons analyzed for U-Pb geochronology are shown on Figures S3A–S3C (see footnote 1). Zircon grains are euhedral, prismatic crystals with average long axes of ~50–150 μm. Most grains display oscillatory zoning. The outermost rims of the dated zircon grains were targeted with ~25 μm ion beam spots to date the youngest crystallization event. Complete U-Pb isotope data can be found in Table S1.

U-Pb zircon ages of the western belt are clustered at 93–115 Ma and 156 Ma (Fig. S1 [see footnote 1] and Table 1). The weighted-mean U-Pb ages (2σ error) of five granitoids from Dibang Valley are 96 ± 3 Ma (PH-1-8-13-1B), 105 ± 3 Ma (PH-1-8-13-3), 94 ± 20 Ma (PH-1-8-13-4B), 93 ± 3 Ma (PH-1-8-13-7), and 115 ± 13 Ma (PH-1-8-13-8). Lohit Valley sample PH-1-5-13-9 yields a U-Pb zircon age of 156 ± 7 Ma (Table 1).

Eastern Lohit Plutonic Complex Belt

The eastern belt of the Lohit Plutonic Complex consists of foliated diorite, garnet-bearing orthogneiss, and migmatite intermingled with marble bands, intruded by younger aplite, pegmatite, and leucogranite (Fig. 6B). Three foliated granitoid samples were collected from Dibang Valley and one from Lohit Valley (Figs. 3 and 5). Granitoids contain quartz, plagioclase, potassium feldspar, biotite, with variable calcic amphibole, garnet, rutile, epidote, and clinozoisite. Cathodoluminescence images of dated zircon grains are shown on Figure S4D (see footnote 1). Zircon grains are typically ~50–100 μm in the longest dimension, transparent in color, and prismatic in shape. Zircon rims were targeted for dating the youngest crystallization age. Complete isotopic age data can be found in Table S2.

The eastern belt samples yield a wider range of U-Pb zircon ages compared to those of the western belt (Fig. S2 [see footnote 1] and Table 1). Sample PH-11-10-15-15 is a garnet-bearing orthogneiss from the middle part of the eastern belt in Dibang Valley (Fig. 3); the sample yields U-Pb zircon ages of 57–95 Ma with a bimodal distribution centered at ca. 70 Ma and ca. 92 Ma, respectively. The weighted-mean age of the entire U-Pb age distribution is 75 ± 9 Ma (Fig. S2A and Table 1).

Orthogneiss sample PH-11-11-15-1 from the northernmost part of the eastern belt (Fig. 3) has a bimodal age distribution between 69 and 165 Ma (Fig. S2B [see footnote 1]). The weighted-mean age of the older age group is 136 ± 5 Ma, whereas the weighted-mean age of the younger group is 69 ± 9 Ma (Fig. S2B).

Sample PH-11-10-15-13 was collected from a migmatitic garnet-bearing orthogneiss unit in the southernmost part of the eastern belt (Fig. 3). Twelve zircon grains from the sample yield $^{207}Pb/^{206}Pb$ ages of 1168–1558 Ma (Tables 1 and S2 [see footnote 1]). Nine other zircon grains produce an age cluster of 1258–1343 Ma with a weighted mean of 1286 ± 14 Ma (Fig. S2C).

Sample PH-1-5-13-5 was collected from a foliated diorite ~1 km east of the Walong thrust in Lohit Valley. Zircon grains from the sample yield a U-Pb zircon age of 101 ± 5 Ma (Fig. S2D [see footnote 1] and Table 1).

Tidding and Mayodia Mélange Complexes

The 8–10-km-thick Tidding and Mayodia mélange complexes are exposed in the hanging wall of the Tidding thrust (Figs. 3, 4B, and 5). Both units were originally mapped as the Tidding suture zone (Nandy, 1973; Thakur and Jain, 1975; Gururajan and Choudhuri, 2003) and the Tidding Formation by Misra (2009). In Dibang Valley, the Mayodia mélange complex is exposed as an incoherent mix of dismembered garnet mica schist, metabasite, chert, amphibolite, gabbro, and serpentinized ultramafics within the Mayodia klippe located near the foreland of the thrust belt (Figs. 4A and 7A). To the north, the Tidding mélange complex consists of amphibolite and chlorite muscovite schist (Figs. 3 and 7B). In Lohit Valley, the Tidding mélange complex consists of a single exposure of incoherently mixed amphibolite and chlorite-muscovite schist in the hanging wall of the Tidding thrust (Fig. 5). Although we mapped the Tidding and Mayodia mélange complexes as separate units based on their map-view separation, we interpret the units to originate from the same complex, which was telescoped across the orogen in the hanging wall of the Tidding thrust and subsequently folded to form an isolated klippe in the foreland (Figs. 3 and 4B).

One chlorite muscovite schist sample (PH-1-9-13-10) from the Mayodia mélange complex (Fig. 4B) yields three youngest zircon ages (±2σ error) of 940 ± 9 Ma, 1326 ± 14 Ma, and 1654 ± 15 Ma (Tables 2 and S3 [see footnote 1]). A wide age population occurs at ~1200–1600 Ma (Fig. 11A). Garnet-mica schist sample PH-1-8-13-26 collected from the Tidding mélange complex in Dibang Valley (Fig. 3) contains age populations of ca. 500–600 Ma, ca. 800 Ma, and ca. 1000 Ma (Fig. 11A), and a youngest zircon age of 40 ± 1 Ma (three grains ≤51 Ma) (Tables 2 and S3).

Mayodia Gneiss

The 1.5–4-km-thick Mayodia gneiss was originally mapped as the Mishmi Crystallines by Gururajan and Choudhuri (2003) and later the Mayodia Group by Misra (2009) (Figs. 3, 4C, and 5). Lithologies include paragneiss, augen gneiss, and quartzofeldspathic schist (Fig. 8A). Meter-wide syntectonic leucogranite dikes intrude the unit near its northernmost exposure (Figs. 3 and 8B). The Mayodia gneiss is in the hanging wall of the north-dipping Demwe thrust, juxtaposed against the Lalpani schist below (Figs. 3, 4C, and 5). In Dibang Valley, the unit is exposed bounding the Mayodia klippe, which originated from the root zone of the Demwe thrust (Figs. 3 and 4B).

Five metasedimentary rocks of the Mayodia gneiss were collected from the basal to uppermost structural sections of the southernmost exposure of the unit in Dibang Valley (Fig. 4C). Mylonitic paragneiss samples PH-1-9-13-19A and PH-1-9-13-19B (located ~50 m upsection) from the basal section of the Mayodia gneiss both contain significant age populations at ca. 1100–1200 Ma, ca. 1300 Ma, and ca. 1400 Ma (Fig. 11B), and Mesoproterozoic youngest ages of 1073 ± 19 Ma (three grains ≤1181 Ma) and 1022 ± 16 Ma (three grains ≤1035 Ma), respectively (Tables 2 and S4 [see footnote 1]).

Augen gneiss sample PH-1-3-13-9, collected from the structural middle section of the unit (Fig. 4C), contains a large ca. 1100 Ma peak and smaller populations at ca. 800 Ma and ca. 1200–1300 Ma (Fig. 11B) and a youngest zircon age of 499 ± 3 Ma (three grains ≤791 Ma) (Tables 2 and S4 [see footnote 1]).

Garnet gneiss sample PH-1-3-13-8, collected from the structurally uppermost section of the Mayodia gneiss (Fig. 4C), contains a strong peak at ca. 1200 Ma, and minor populations at ca. 1100 Ma, ca. 1300–1400 Ma (Fig. 11B), and a youngest zircon age of 1069 ± 13 Ma (three grains ≤1079 Ma) (Tables 2 and S4 [see footnote 1]). Schist sample PH-1-3-13-10A, collected upsection from PH-1-3-13-8 (Fig. 4C), contains age populations at ca. 800 Ma, ca. 1100–1200 Ma, ca. 1300–1400 Ma, and ca. 1700 Ma (Fig. 11A) and a Neoproterozoic youngest zircon age of 646 ± 13 Ma (three grains ≤841 Ma) (Tables 2 and S4).

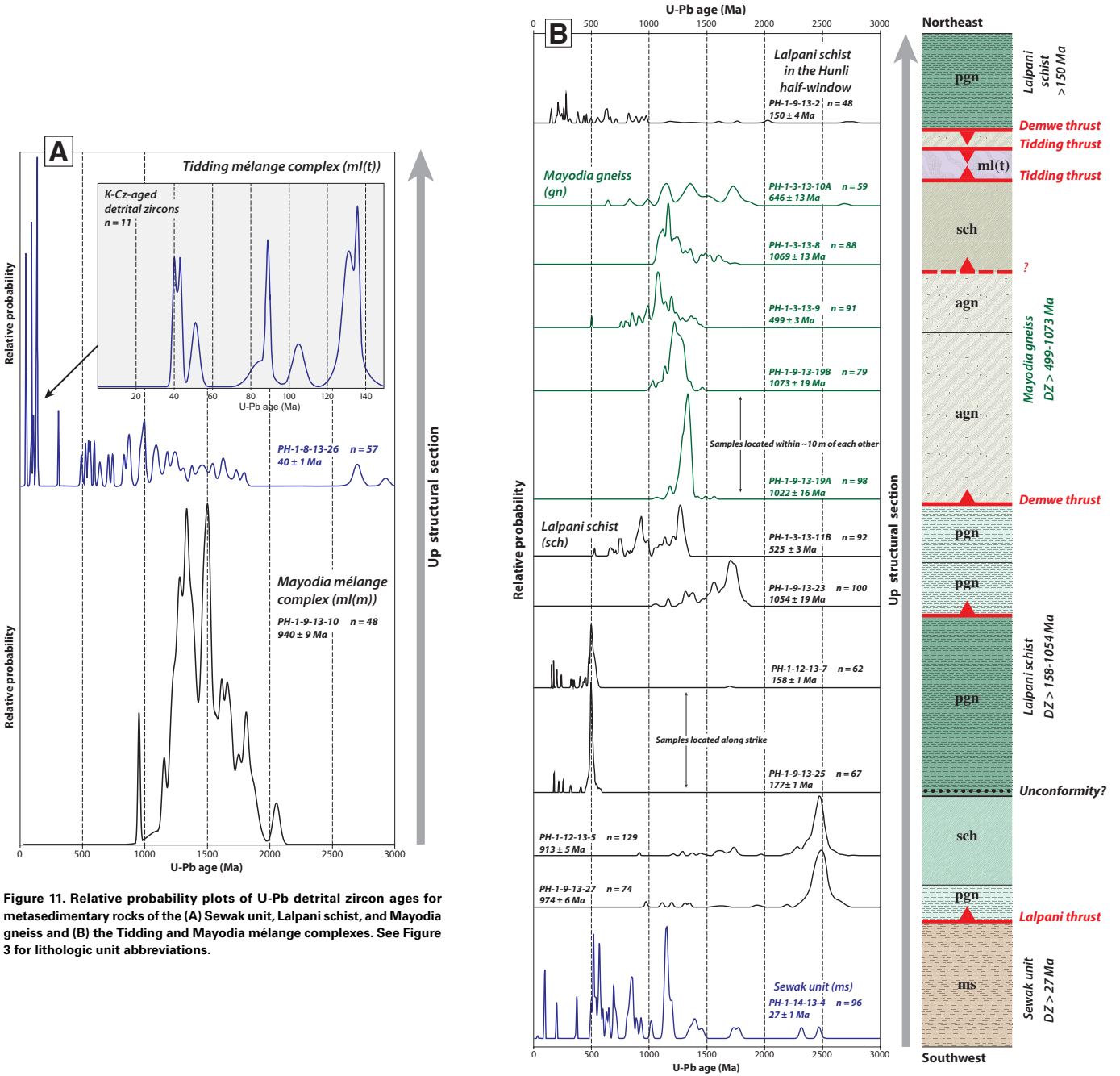

Figure 11. Relative probability plots of U-Pb detrital zircon ages for metasedimentary rocks of the (A) Sewak unit, Lalpani schist, and Mayodia gneiss and (B) the Tidding and Mayodia mélange complexes. See Figure 3 for lithologic unit abbreviations.

Lalpani Schist

The Lalpani schist is exposed in both Lohit and Dibang Valleys (Figs. 3, 4C, and 5) and consists of quartzofeldspathic schist, paragneiss, quartzite, and carbonate, intruded in some locations by meter-wide mafic dikes (Fig. 9). The unit was originally mapped as the lower section of the Mishmi Crystallines by Gururajan and Choudhuri (2003) and later the Lalpani Group by Misra (2009).

Seven samples of the Lalpani schist were collected for U-Pb zircon geochronology (Figs. 3 and 4C). The youngest U-Pb zircon ages from the samples range from Mesoproterozoic for the basal unit to Cretaceous in the uppermost section, signaling changes in the source areas (Fig. 11A). Two quartzofeldspathic paragneiss samples, PH-1-12-13-5 and PH-1-9-13-27 from the basal section of the Lalpani schist, ~9 km apart from one another along strike (Fig. 4C), yield nearly identical U-Pb age spectra with a significant peak at ca. 2500 Ma (Fig. 11B) and a youngest individual zircon age of 913 ± 5 Ma (three grains ≤1572 Ma) and 974 ± 6 Ma (three grains ≤1195 Ma), respectively (Tables 2 and S5 [see footnote 1]).

Schist sample PH-1-9-13-23 is structurally higher than the previous two samples (Fig. 4C) and yields zircon populations of ca. 1100–1200 Ma, ca. 1400 Ma, and ca. 1600 Ma (Fig. 11B). The youngest individual zircon age was 1054 ± 19 (three grains ≤1166 Ma) (Tables 2 and S5 [see footnote 1]).

Paragneiss sample PH-1-3-13-11B, collected from the upper-middle structural section of the Lalpani schist (Fig. 4C), contains zircon grains with Mesoproterozoic to Cambrian ages clustered at ca. 1300 Ma, ca. 800–900 Ma, and ca. 700 Ma (Fig. 11B). The sample yields a youngest age of 525 ± 3 Ma (three grains ≤668 Ma) (Tables 2 and S5 [see footnote 1]).

Samples PH-1-12-13-7 and PH-1-9-13-25 are mylonitic quartzofeldspathic paragneiss collected from the lowermost structural section of the Lalpani schist (Fig. 4C). Both samples yield identical U-Pb age spectra, with a strong peak at ca. 500 Ma (Fig. 11A) and youngest zircon ages of 158 ± 1 Ma and 177 ± 1 Ma, respectively (Tables 2 and S5 [see footnote 1]).

Schist sample PH-1-9-13-2, collected from the Hunli half-window (Fig. 3), yields a youngest zircon age of 150 ± 4 Ma (three grains ≤200 Ma), like samples PH-1-12-13-7 and PH-1-9-13-25 (Tables 2 and S5 [see footnote 1]). However, sample PH-1-9-13-2 has a larger distribution of U-Pb ages with populations at ca. 150–350 Ma, ca. 400 Ma, ca. 500–700 Ma, and ca. 800–1000 Ma (Fig. 11A).

Tezu Unit

The Tezu unit is a ~2-km-thick sequence of non-marine, syntectonic strata including interbedded conglomerate, coarse-grained sandstone, and mudstone (Fig. 10A). The unit was observed in only one location along the range front, directly northwest of Lohit Valley (Fig. 5). Conglomeratic layers are defined by cobble-sized clasts exposed in meter-wide channels within a sandy matrix. The north-dipping Tezu unit section is oriented right-way-up, evidenced by normal grading and conglomeratic channels. The Tezu unit is in the footwall of the Lalpani thrust, juxtaposed against the Lalpani schist (Fig. 5). U-Pb detrital zircon geochronology was not performed on samples from this unit.

Sewak Unit

The Sewak unit, which was originally mapped by Misra (2009) as the Sewak Group, consists of a ~1.5-km-thick section of low-grade metasedimentary rocks including interbedded quartzite, marble, chert, slate, phyllite, and quartzofeldspathic schist (Fig. 10B). The unit is exposed along the range front in the hanging walls of the Tezu thrust in Lohit Valley and Mishmi thrust in Dibang Valley (Figs. 3, 4C, and 5). In Dibang Valley, the Sewak unit is the southernmost lithologic unit thrust atop Quaternary alluvium by the active Mishmi thrust (Figs. 3 and 4C).

Phyllite sample PH-1-14-13-4 from the middle structural level of the Sewak unit (Fig. 4C) yields a single youngest zircon age of 27 ± 1 Ma, with three spot analyses of ≤30 Ma (Tables 2 and S6 [see footnote 1]). The sample displays prominent zircon age populations of ca. 90 Ma, ca. 130 Ma, ca. 500–600 Ma, ca. 800 Ma, and ca. 1100–1200 Ma (Fig. 11B).

RESULTS OF WHOLE-ROCK GEOCHEMISTRY

Plutonic Rocks

The Lohit Plutonic Complex consists of predominantly calc-alkaline diorite suite rocks featuring both I- and S-type major- and/or trace-element signatures (Figs. 12A, 13A, and S5 and Table S7 [see footnote 1]). All granitoid samples are peraluminous diorites with high Al_2O_3 (>19 wt%), A/CNK values (>1.58), A/NK (>2.75), and Rb (>100 ppm) (Fig. 12B and Table S7). One sample from the eastern Lohit Plutonic Complex belt (PH-11-10-15-13) is a garnet-bearing, low-K granodiorite (Fig. 12A and Table S7).

Trace-element signatures of five samples of the Lohit Plutonic Complex are consistent with volcanic arc origins, along with generation in an orogenic setting (Pearce et al., 1984) (Fig. 13B). Rare-earth element concentrations of four granitoids reflect moderate to high fractionation between heavy rare-earth elements (HREEs) and light rare-earth elements (LREEs) (La/Yb: ~7–15) (Figs. S5 and S6 and Table S7). One granitoid intrusion of the Tidding mélange complex (PH-1-8-13-22) is a metaluminous diorite based on moderate to high Na_2O (>3.75 wt%), high CaO (>5.8 wt%), low Rb (<35 ppm), and coexisting hornblende and sphene (Table S7).

Mafic and Ultramafic Rocks

Five mafic samples collected from the Mayodia mélange complex and mafic dikes in the Mayodia gneiss and Lohit Plutonic Complex yield compositions

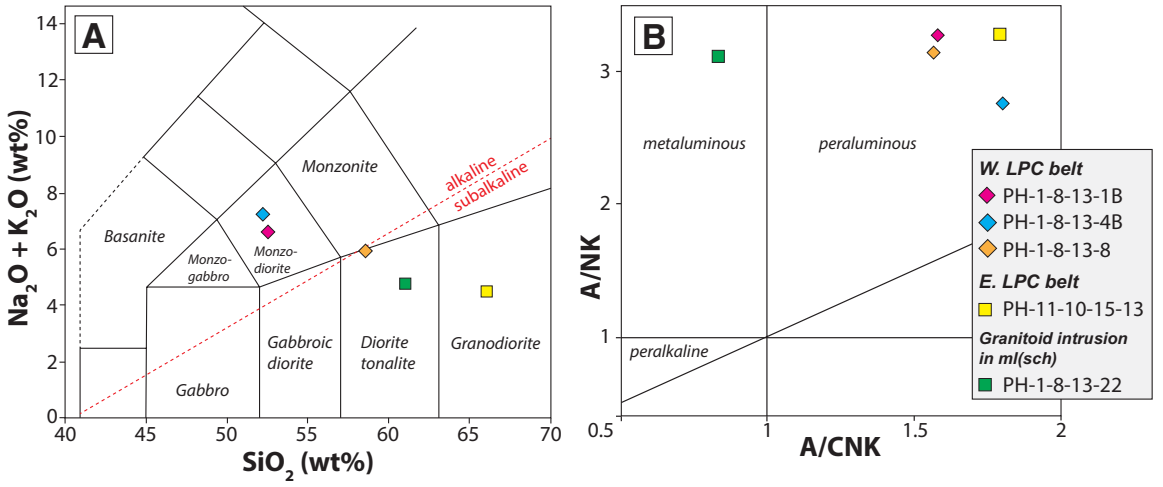

Figure 12. Geochemical plots for plutonic rocks including (A) alkalis versus silica classification and (B) $Al_2O_3/N_2O + K_2O$ versus $Al_2O_3/CaO + N_2O + K_2O$. Plots are based on the methods of Shand (1943) and Le Bas et al. (1986). LPC—Lohit Plutonic Complex.

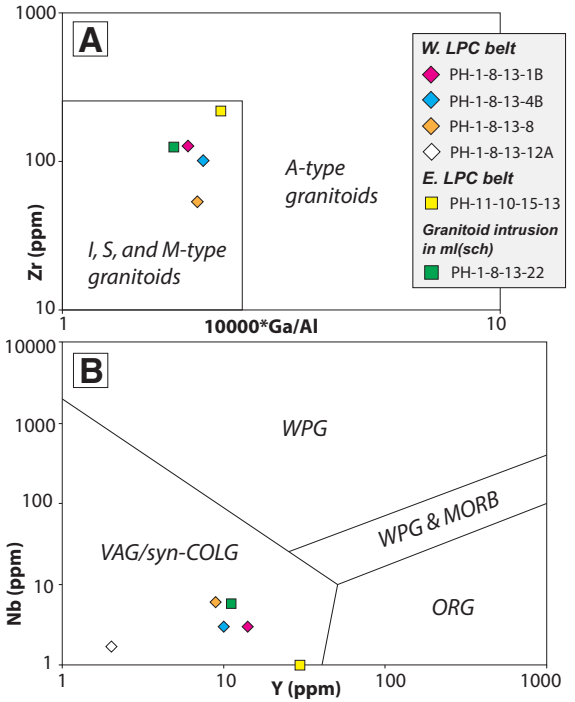

Figure 13. Diagrams of (A) source for plutonic rocks including anorogenic (A), igneous (I), sedimentary (S), and mantle (M) types based on Zr versus 10,000*Ga/Al and (B) tectonic settings diagrams for plutonic rocks including syncollisional (syn-COLG), within-plate granite (WPG), volcanic arc granite (VAG), orogenic (ORG) based on Nb versus Y. Plots are based on the methods of Pearce et al. (1984). LPC—Lohit Plutonic Complex.

ranging from basalt and basaltic andesite on a SiO_2 versus total alkalis diagram (Le Bas et al., 1986) (Fig. 14A). One sample (PH-1-9-13-7B) from the Mayodia mélange complex contains stichtite and SiO_2 <45%, implying the presence of ultramafic blocks within the mélange (Fig. 14A and Table S8). Seven mafic samples predominantly fall in the mid-ocean ridge basalt (MORB) (Figs. 14B and S7) and oceanic-arc fields on trace-element discriminant diagrams (Nb/La versus La/Yb; V versus Ti; Ti versus Zr; Cr versus Y; Zr/Y versus Zr) (Pearce, 1982; Shervais, 1982; Condie, 1989) (Fig. S7 and Table S8). Mafic rock samples display relatively flat trace-element slopes (La/Yb: ~1.5–4) on a spider diagram, in contrast to sample PH-1-9-13-7B interpreted to have an ultramafic protolith (La/Yb: ~9) (Fig. S8 and Table S8).

Sr and Nd Isotope Geochemistry

Neodymium and strontium isotopic compositions aid in differentiating protoliths of the LHS from the GHC (e.g., Parrish and Hodges, 1996; Huyghe et al., 2001; Robinson et al., 2001; Aikman et al., 2012a) and identifying the

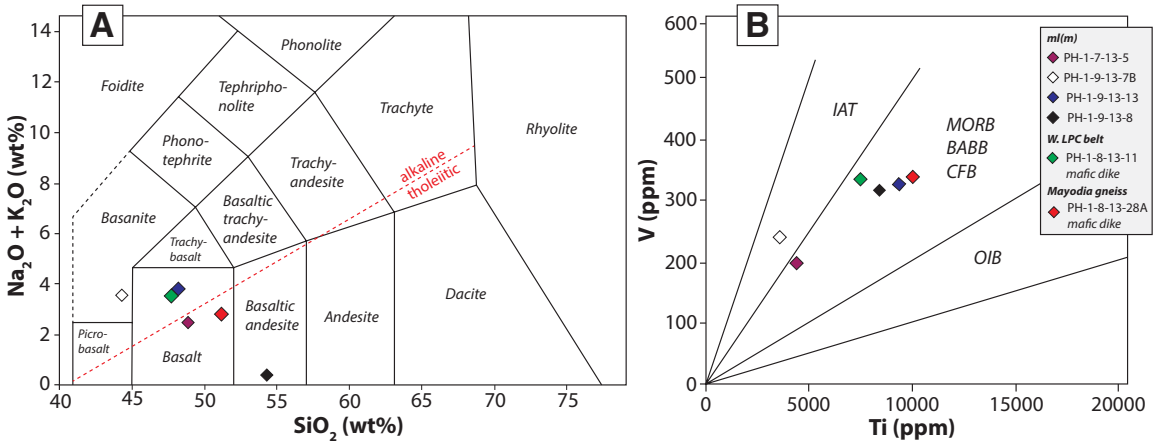

Figure 14. Diagrams of (A) alkalis versus silica concentrations in mafic and ultramafic rocks (Le Bas et al., 1986) and (B) tectonic setting including mid-ocean ridge basalts (MORB), oceanic island basalts (OIB), backarc basins basalts (BABB), island arc tholeiites (IAT), and continental arc or flood basalts (CFB) based on V versus Ti. Plots are based on the methods of Pearce (1982), Shervais (1982), and Condie (1989). LPC—Lohit Plutonic Complex.

source and evolution of igneous rocks (e.g., Kistler and Ross, 1990; Chung et al., 1998). We determined the isotopic ratios of $^{143}Nd/^{144}Nd$ (normalized to chondritic uniform reservoir [CHUR] in epsilon notation) and initial $^{87}Sr/^{86}Sr$ (Sr_i) for igneous rocks of the western Lohit Plutonic Complex belt (Figs. 15 and 16) and Tidding and Mayodia mélange complexes to understand source and setting of magmagenesis (Fig. 16). $^{143}Nd/^{144}Nd$ and Sr_i ratios were determined for the Mayodia gneiss, Lalpani schist, and Sewak unit to test correlation with the GHC and LHS of the Himalaya orogen (Fig. 16). Results of Sr and Nd isotopic analyses are summarized in Table 3.

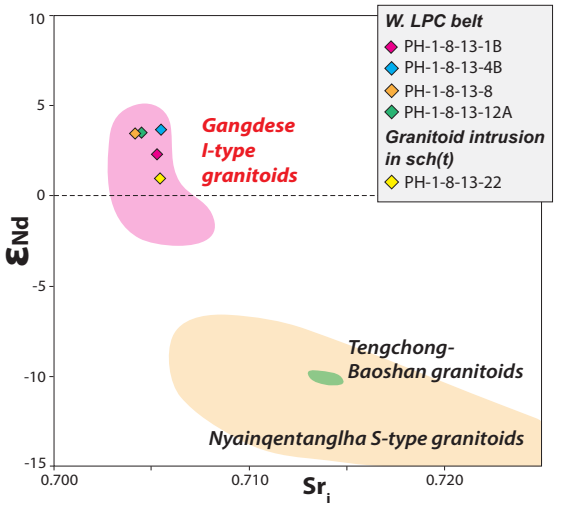

Figure 15. Plot of ε_{Nd} versus Sr_i ($^{87}Sr/^{86}Sr$) depicting granitoids of the western Lohit Plutonic Complex (LPC) belt within the Gangdese I-type granitoid field, adapted from Mitchell et al. (2012).

Five granitoid samples from the western Lohit Plutonic Complex belt yield positive ε_{Nd} values of 2.2–5.1 and Sr_i values of 0.704–0.705 (Figs. 15 and 16), comparable to those of I-type Gangdese granitoids of the southern Lhasa terrane (Fig. 15). Three samples from the Mayodia mélange complex, located near the Tidding thrust, yield positive ε_{Nd} values of 5.0–7.7 and Sr_i of 0.704–0.706, whereas two samples of the Tidding mélange complex near the Lohit thrust contain ε_{Nd} values of –7.2 and 0.8 and Sr_i values of 0.706–0.712 (Fig. 16). Four samples from the Mayodia gneiss yield ε_{Nd} values between –17.5 and –10.3 and Sr_i values of 0.715–0.912 (Fig. 16). Three Lalpani schist samples yield negative ε_{Nd} values of –27.8 to –16 (Fig. 16), indicative of a Lesser Himalayan affinity. The same Lalpani schist samples have Sr_i values between 0.709 and 0.895 (Fig. 16). One Lalpani schist sample collected from the Hunli window (Fig. 3) has a less negative ε_{Nd} value of –5.5 and Sr_i of 0.709 (Fig. 16). One phyllite sample of the Sewak unit has a ε_{Nd} value of –10.2 and Sr_i of 0.712 (Fig. 16).

REGIONAL CORRELATION OF LITHOLOGIC UNITS

Our results allow us to correlate the major rock units of the northern Indo-Burma Ranges with those of the Himalaya orogen and the Lhasa terrane (Fig. 2). As detailed below, several Himalayan-Tibetan lithologic units are missing in the study area, which implies either a unique tectonic process controlled the development of the northern segment of the Eastern Flanking Belt or possibly a greater magnitude of crustal shortening and/or continental underthrusting occurred across the study area compared to the Himalayan orogen to the west (Fig. 17).

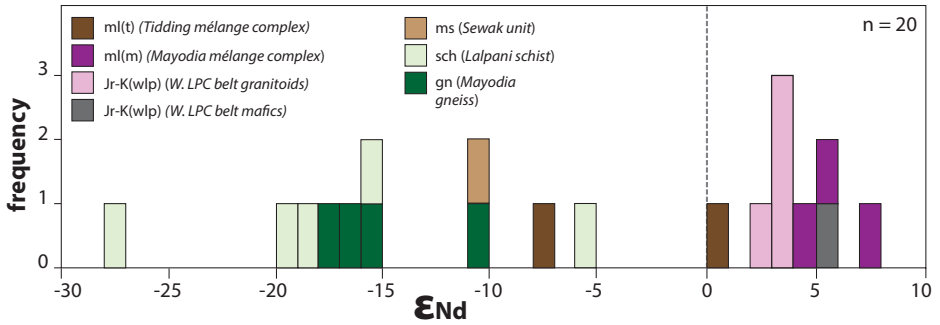

Figure 16. Plot of the frequency of ε_{Nd} values for all samples. LPC—Lohit Plutonic Complex.

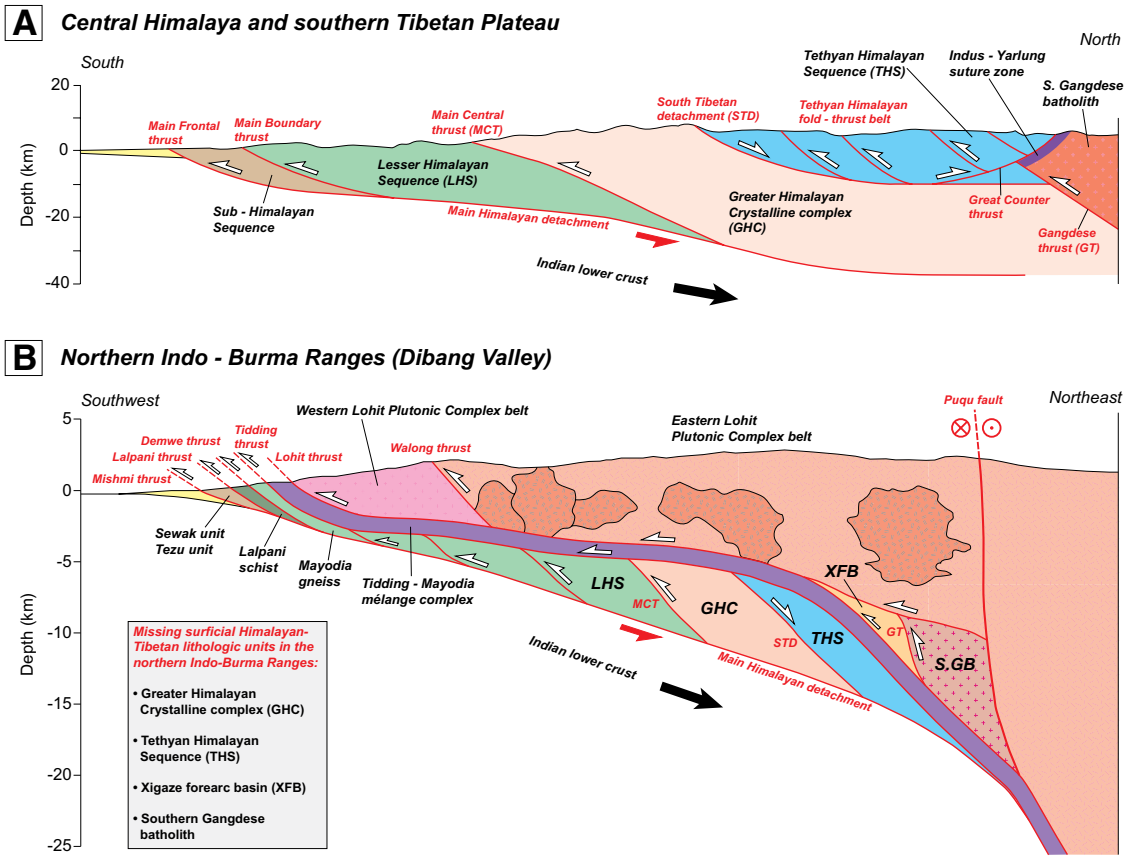

Figure 17. Schematic geologic cross sections across (A) the central Himalaya-southern Tibetan Plateau and (B) the northern Indo-Burma Ranges showing correlation of major lithologic units. GB—Gangdese batholith.

Sub-Himalayan Sequence

The Sewak unit and Tezu units are the structurally lowest rocks exposed in the study area (Fig. 2). The Sewak unit is comparable to the Sub-Himalayan Sequence based on structural position, and the presence of young zircon ages of <30 Ma in both the Sub-Himalayan Sequence and Sewak unit (Fig. 11B) strengthens this correlation (Yin, 2006) (Fig. 2). However, we note that the presence of low-grade metamorphic rocks in the Sewak unit makes it different than the Sub-Himalayan Sequence.

The Tezu unit has a similar lithology to that of the Miocene–Pliocene Siwalik Group in the Sub-Himalayan Sequence (e.g., DeCelles et al., 1998). The structural position of the Tezu unit atop the Indian foreland basin by an active, range-bounding fault (i.e., Mishmi thrust) is also like that of the Sub-Himalayan Sequence (Yin, 2006) (Fig. 2).

Lesser Himalayan Sequence and Greater Himalayan Crystalline Complex

Because both the LHS and GHC consist of medium- to high-grade metamorphic rocks, differentiating the units without a clear structural context can be challenging. The strike-slip faults bounding the eastern Himalayan syntaxis (Fig. 1C) prevent the testing of the along-strike continuity of major thrusts between the northern Indo-Burma Ranges and Himalayan orogen. However, we compared U-Pb detrital zircon ages between lithologic units (Gehrels et al., 2011) using the nonparametric K-S statistical test for the Mayodia gneiss, Lalpani schist, LHS, and GHC. The tests were conducted using the Excel macro generated by George Gehrels at the University of Arizona LaserChron Center (https://sites.google.com/a/laserchron.org/laserchron/). In the test, the observed vertical difference (D_{obs}) between the cumulative probability distributions is compared to a critical value (D_{crit}), determined from the number of zircon analyses per sample. In this study, a maximum D_{obs} value of 0.05 is established. If the D_{obs} is greater than D_{crit}, the null hypothesis that the samples are derived from the same source can be rejected. The *P* value is the maximum value of the significance level at which the null hypothesis can be accepted. If the *P* value is greater than 0.05, then the zircon age distributions are derived from the same source at the 95% confidence level. Results of the K-S statistical test are summarized in Table S9 (see footnote 1).

The test shows that schist sample PH-1-3-13-10A of the Mayodia gneiss is similar with rocks of the Arunachal Himalaya, specifically sample AY 02-13-06-7 of the GHC (Webb et al., 2013) and sample AY9160314A of the LHS (Yin et al., 2006) (Table S9 [see footnote 1]). However, sample AY 02-13-06 from the Arunachal Himalaya is located within the Main Central thrust shear zone, which in some locations extends into the upper LHS (Yin, 2006). We interpret the Mayodia gneiss to correlate with the LHS based on the similarity of detrital zircon ages with sample AY9160314A, comparable metamorphic lithologies, and similar negative ε_{Nd} values of –17.5 to –10.3 (Fig. 16 and Table 3). Furthermore, the Mayodia gneiss lacks (1) ca. 870 Ma and ca. 500 Ma orthogneiss; (2) large leucogranite sheets or laccolith bodies (e.g., Arunachal and Tsona leucogranites); and (3) significant U-Pb detrital zircon age populations at ca. 540–750 Ma and ca. 800–1200 Ma (Fig. 11B), all of which are common in the GHC (Yin et al., 2010a; Gehrels et al., 2011; Aikman et al., 2012a, 2012b; Webb et al., 2013; Harrison and Wielicki, 2016). Similarly, the Lalpani schist is correlated to the LHS based on (1) similar lithologies and metamorphic grades; (2) negative ε_{Nd} values mostly between –27.8 and –16 (Fig. 16 and Table 3); and (3) the presence of the Mesoproterozoic–Cambrian detrital zircon ages (Fig. 11B).

Indus-Yarlung Suture Zone

The Tidding and Mayodia mélange complexes are interpreted to originate from the same complex, which correlates with the Indus-Yarlung suture zone. This is based on (1) the exposure of amalgamated basalts, gabbro, ultramafics, and mafic schist of a dismembered ophiolite sequence within the Tidding-Mayodia mélange complex; (2) generation of igneous rocks in a mid-ocean ridge setting (Fig. 14B); and (3) the position of the mélange complex between rocks of Indian and Lhasa terrane affinities (Figs. 3 and 5). Metasedimentary rocks containing Eocene zircons (ca. 40 Ma) (Fig. 11A) could have been part of a syntectonic basin within the suture zone.

Mesozoic Magmatic Arc and Mesoproterozoic Basement of the Lhasa Terrane

Following the interpretation of Lin et al. (2013), we suggest that the Lohit Plutonic Complex is the southeastward continuation of the Mesozoic Cenozoic northern Gangdese batholith belt based on (1) similar Jurassic–Cretaceous crystallization ages between ca. 69–156 Ma (Table 1); (2) low Th/Y and La/Yb ratios in I-type granitoids (Fig. 13A); (3) trace-element signatures indicating volcanic arc origins (Fig. 13B); (4) Sr_i values of ≤0.705 (Fig. 15 and Table 3); (5) positive ε_{Hf} values (10–14) (Lin et al., 2013); and (6) positive ε_{Nd} values (Figs. 15 and 16 and Table 3). Furthermore, similar Cretaceous zircon ages along with ε_{Nd} and Sr_i values are found in the Wuntho-Popa and Mogok Metamorphic belts to the south (Mitchell, 1993; Mitchell et al., 2012; Wang et al., 2014). The existence of a continuous magmatic arc stretching from the southern Lhasa terrane to the West Burma block and Sibumasu plate supports the model of continuous Neotethys subduction and Andean-type magmatism along an elongated boundary (Lin et al., 2013).

The eastern Lohit Plutonic Complex belt is distinct in having both Cretaceous (ca. 69–136 Ma) and Mesoproterozoic (ca. 1286 Ma) zircons (Table 1). The ca. 1286 Ma orthogneiss correlates with the Bomi-Chayu Complex (1276–1342 Ma), which is exposed surrounding the eastern Himalayan syntaxis (Xu et al., 2013) (Fig. 1C). The Bomi-Chayu Complex is notable for being the oldest rocks exposed in the Lhasa terrane (Xu et al., 2013), and our observations suggest

that these rocks extend southeast to the northern Indo-Burma Ranges in the hanging wall of the Walong thrust (Fig. 1C).

Absence of Cenozoic plutonic and volcanic rocks (e.g., analogous to the Linzizong volcanics) of the southern Gangdese batholith belt in the study area raises the question of whether Cenozoic magmatism was occurring along the entire southern Lhasa margin during the Cenozoic. Existing research has shown that ca. 50–55 Ma mafic rocks of Gangdese affinity are exposed in the Mogok Metamorphic Belt of northwest Yunnan to the south of the study area (e.g., Wang et al., 2014). Furthermore, Eocene–Oligocene granitoids and Miocene–Quaternary volcanic flows related to Neotethys subduction are exposed throughout the Wuntho-Popa belt in present-day Myanmar (Mitchell, 1993; Mitchell et al., 2012; Lee et al., 2016). The existence of Cenozoic subduction-generated rocks both to the northwest and south of the study area suggests Cenozoic magmatism did occur in the northern Indo-Burma Ranges, but these igneous rocks may have been shortened and eroded and/or underthrusted during development of the orogen (Fig. 17).

DISCUSSION

Correlation of the Lalpani schist and Mayodia gneiss with the LHS (Fig. 2) suggests that prior to the Cenozoic India-Asia collision, rocks comprising the northeast Indian cratonal sequence extended to the east and southeast of the present-day location of the eastern Himalayan syntaxis. Rocks of the Indian passive continental margin (i.e., THS) and Indian cratonal sequence (i.e., GHC and LHS) would have existed along the northeast margin of the Greater Indian continent. The existence of Late Jurassic–Cretaceous granitoids within the study area that are equivalent to the northern Gangdese batholith belt implies that subduction of Neo-Tethys oceanic lithosphere and arc magmatism occurred along a continuous belt encompassing both the southern Lhasa terrane and Eastern Flanking Belt (e.g., Lin et al., 2013). Following initial India-Asia collision, Cenozoic magmatism (i.e., southern Gangdese batholith belt) also occurred along an elongated belt from the southern Lhasa terrane to the Eastern Flanking Belt. An accompanying Mesozoic–Cenozoic forearc basin was likely present along the entire Neo-Tethys subduction margin.

We interpret the absence of these major Himalayan-Tibetan units in the northern Indo-Burma Ranges to result from a greater magnitude of (1) Cenozoic shortening and erosion compared to the Himalayan orogen to the west and/or (2) continental underthrusting. Haproff et al. (2018) showed that the south- to west-directed northern Indo-Burma thrust belt accommodated clockwise rotation of Himalayan-Tibetan rocks around the eastern Himalayan syntaxis. Progressive clockwise rotation of the thrust belt from an originally east-trending configuration implies a spatial gradient in shortening strain, such that the magnitude of crustal shortening increases with distance from the pole of rotation at the eastern Himalayan syntaxis. This interpretation is supported by the dramatic southward decrease in the map-view distance between the active foreland basin and Tidding mélange complex (= IYSZ), which is ~33 km along Dibang Valley and ~5 km along Lohit Valley farther to the southeast. For comparison, the map-view distance between the Main Frontal thrust and IYSZ across the western Arunachal Himalaya, perpendicular to the strike of the orogen, is ~200 km (Yin et al., 2010a). This width of the thrust belt decreases to ~5 km over a map-view distance of ~250 km to the south of the eastern Himalayan syntaxis (Fig. 1). Upper-plate shortening at the longitude of the northern Indo-Burma Ranges may also have been coeval with the underthrusting of complete sections of Greater India and southern Lhasa terrane. In this case, the Tethyan Himalayan thrust belt, GHC, Xigaze forearc basin, and southern Gangdese batholith belt were underthrusted together with the Indian continent below the southeastern Tibetan Plateau (Fig. 17).

CONCLUSIONS

Our study presents the results of U-Pb zircon geochronology and whole-rock geochemistry of lithologic units exposed in the northern Indo-Burma Ranges, located east to southeast of the eastern Himalayan syntaxis. Geochronological and geochemical data were coupled with lithologic and structural observations to test the lateral continuity of rocks of the easternmost Himalayan collisional system. We infer that lithologic units exposed in the study area are the easternmost continuations of the Cenozoic Sub-Himalayan Sequence, Lesser Himalayan Sequence, and Indus-Yarlung suture zone. The eastern Lohit Plutonic Complex contains Mesoproterozoic basement rocks of the Lhasa terrane (i.e., Bomi-Chayu Complex), whereas the western Lohit Plutonic Complex belt correlates with the Mesozoic northern Gangdese batholith belt. Based on comparable U-Pb zircon ages and geochemical composition between the Gangdese batholith and Lohit Plutonic Complex, subduction of Neotethys oceanic lithosphere, Mesozoic arc magmatism, and forearc basin sedimentation occurred along a continuous belt encompassing the southern Lhasa terrane and Eastern Flanking Belt along the southern margin of Asia. Prior to the early Cenozoic India-Asia collision, the northeast continental margin of Greater India was likely a continuous sequence involving rocks of the Lesser Himalayan Sequence, Greater Himalayan Crystalline Complex, and the Tethyan Himalayan Sequence. Once collision initiated, rocks of the Himalayan orogen and southern Lhasa terrane experienced coeval clockwise rotation and shortening around northeast India; this rotation was accommodated by a south- to west-directed thrusting. During progressive development of the northern Indo-Burma thrust belt, a greater magnitude of crustal shortening and/or continental underthrusting occurred as compared to the Himalayan orogen to the west, resulting in local complete erosion and/or underthrusting of several Himalayan-Tibetan lithologic units.

ACKNOWLEDGMENTS

This work is supported by a grant from the Tectonics Program of U.S. National Science Foundation. We thank editor Raymond Russo, Peter Zeitler, and an anonymous reviewer for their constructive comments.

REFERENCES CITED

Acharyya, S.K., 1980, Stratigraphy and tectonics of Arunachal Lesser Himalaya, *in* Bhatia, S.B., and Valdiya, K.S., eds., Stratigraphy and Correlations of Lesser Himalayan Formations: Delhi, India, Hindustan Publishing, p. 231–241.

Acharyya, S.K., 1987, Cenozoic plate motions creating the Eastern Himalayan and Indo Burmese range around the northeast corner of India in Ghosh, N.C., and Varadrajan, S., eds., Amphibolites and Indian Plate Margins: Patna, India, Patna University, p. 143–160.

Acharyya, S.K., 1994, The Cenozoic foreland basin and tectonics of the eastern sub-Himalaya: problems and prospects: Himalayan Geology, v. 15, p. 3–21.

Acharyya, S.K., and Ray, K.K., 1977, Geology of the Darjeeling-Sikkim Himalaya: Guide to Excursion No. 3: Fourth International Gondwana Symposium, Calcutta, p. 1–25.

Aikman, A.B., Harrison, T.M., and Lin, D., 2008, Evidence for early (>44 Ma) Himalayan crustal thickening, Tethyan Himalaya, southeastern Tibet: Earth and Planetary Science Letters, v. 274, no. 1, p. 14–23, https://doi.org/10.1016/j.epsl.2008.06.038.

Aikman, A.B., Harrison, T.M., and Hermann, J., 2012a, Age and thermal history of Eo- and Neohimalayan granitoids, eastern Himalaya: Journal of Asian Earth Sciences, v. 51, p. 85–97, https://doi.org/10.1016/j.jseaes.2012.01.011.

Aikman, A.B., Harrison, T.M., and Hermann, J., 2012b, The origin of Eo- and Neo-himalayan granitoids, Eastern Tibet: Journal of Asian Earth Sciences, v. 58, p. 143–157, https://doi.org/10.1016/j.jseaes.2012.05.018.

Aitchison, J.C., Ali, J.R., and Davis, A.M., 2007, When and where did India and Asia collide?: Journal of Geophysical Research. Solid Earth, v. 112, B05423, https://doi.org/10.1029/2006JB004706.

Allégre, C.O., Courtillot, V., Tapponnier, P., Hirn, A., Mattauer, M., Coulon, C., Jaeger, J.J., Achache, J., Schärer, U., Marcoux, J., and Burg, J.P., 1984, Structure and evolution of the Himalaya-Tibet orogenic belt: Nature, v. 307, no. 5946, p. 17–22, https://doi.org/10.1038/307017a0.

An, W., Hu, X., Garzanti, E., BouDagher-Fadel, M.K., Wang, J., and Sun, G., 2014, Xigaze forearc basin revisited (South Tibet): Provenance changes and origin of the Xigaze Ophiolite: Geological Society of America Bulletin, v. 126, no. 11–12, p. 1595–1613, https://doi.org/10.1130/B31020.1.

Bhargava, O.N., 1995, The Bhutan Himalaya, a geological account: Geological Survey of India Bulletin, no. 39, 245 p.

Burchfiel, B.C., Zhiliang, C., Hodges, K.V., Yuping, L., Royden, L.H., Changrong, D., and Jiene, X., 1992, The South Tibetan detachment system, Himalayan orogen: Extension contemporaneous with and parallel to shortening in a collisional mountain belt: Geological Society of America Special Paper 269, 41 p., https://doi.org/10.1130/SPE269-p1.

Burgess, W.P., Yin, A., Dubey, C.S., Shen, Z.K., and Kelty, T.K., 2012, Holocene shortening across the Main Frontal Thrust zone in the eastern Himalaya: Earth and Planetary Science Letters, v. 357, p. 152–167, https://doi.org/10.1016/j.epsl.2012.09.040.

Cai, F., Ding, L., Leary, R.J., Wang, H., Xu, Q., Zhang, L., and Yue, Y., 2012, Tectonostratigraphy and provenance of an accretionary complex within the Yarlung-Zangpo suture zone, southern Tibet: Insights into subduction-accretion processes in the Neo-Tethys: Tectonophysics, v. 574, p. 181–192, https://doi.org/10.1016/j.tecto.2012.08.016.

Chang, C.F., and Zheng, X.L., 1973, Tectonic features of the mount Jolmo Lungma region in southern Tibet, China: Chinese Journal of Geology, v. 1, p. 1–12.

Chung, S.L., Lo, C.H., Lee, T.Y., Zhang, Y., Xie, Y., Li, X., Wang, K.L., and Wang, P.L., 1998, Diachronous uplift of the Tibetan plateau starting 40 Myr ago: Nature, v. 394, no. 6695, p. 769–773, https://doi.org/10.1038/29511.

Clark, M.K., and Bilham, R., 2008, Miocene rise of the Shillong Plateau and the beginning of the end for the Eastern Himalaya: Earth and Planetary Science Letters, v. 269, no. 3, p. 337–351, https://doi.org/10.1016/j.epsl.2008.01.045.

Cobbold, P.R., and Davy, P.H., 1988, Indentation tectonics in nature and experiment. 2. Central Asia: Bulletin of the Geological Institution of the University of Upsala, v. 14, p. 143–162.

Condie, K.C., 1989, Geochemical changes in basalts and andesites across the Archean-Proterozoic boundary: Identification and significance: Lithos, v. 23, no. 1–2, p. 1–18, https://doi.org/10.1016/0024-4937(89)90020-0.

Copeland, P., Harrison, T.M., Yun, P., Kidd, W.S.F., Roden, M., and Zhang, Y., 1995, Thermal evolution of the Gangdese batholith, southern Tibet: A history of episodic unroofing: Tectonics, v. 14, no. 2, p. 223–236, https://doi.org/10.1029/94TC01676.

Corrie, S.L., Kohn, M.J., McQuarrie, N., and Long, S.P., 2012, Flattening the Bhutan Himalaya: Earth and Planetary Science Letters, v. 349, p. 67–74, https://doi.org/10.1016/j.epsl.2012.07.001.

Coulon, C., Maluski, H., Bollinger, C., and Wang, S., 1986, Mesozoic and Cenozoic volcanic rocks from central and southern Tibet: ^{39}Ar-^{40}Ar dating, petrological characteristics and geodynamical significance: Earth and Planetary Science Letters, v. 79, no. 3, p. 281–302, https://doi.org/10.1016/0012-821X(86)90186-X.

Coward, M.P., Kidd, W.S.F., Yun, P., Shackleton, R.M., and Hu, Z., 1988, The structure of the 1985 Tibet geotraverse, Lhasa to Golmud: Philosophical Transactions of the Royal Society of London A: Mathematical, Physical and Engineering Sciences, v. 327, no. 1594, p. 307–333.

Dai, J., Wang, C., Hébert, R. Li, Y., Zhong, H., Guillaume, R., Bezard, R., and Wei, Y., 2011a, Late Devonian OIB alkaline gabbro in the Yarlung Zangbo suture zone: Remnants of the Paleo-Tethys?: Gondwana Research, v. 19, no. 1, p. 232–243, https://doi.org/10.1016/j.gr.2010.05.015.

Dai, J.G., Wang, C.S., Hébert, R., Santosh, M., Li, Y.L., and Xu, J.Y., 2011b, Petrology and geochemistry of peridotites in the Zhongba ophiolite, Yarlung Zangbo Suture Zone: Implications for the Early Cretaceous intra-oceanic subduction zone within the Neo-Tethys: Chemical Geology, v. 288, no. 3, p. 133–148, https://doi.org/10.1016/j.chemgeo.2011.07.011.

Daniel, C.G., Hollister, L.S., Parrish, R.T., and Grujic, D., 2003, Exhumation of the Main Central Thrust from lower crustal depths, eastern Bhutan Himalaya: Journal of Metamorphic Geology, v. 21, no. 4, p. 317–334, https://doi.org/10.1046/j.1525-1314.2003.00445.x.

Davidson, C., Crujic, D.E., Hollister, L.S., and Schmid, S.M., 1997, Metamorphic reactions related to decompression and synkinematic intrusion of leucogranite, High Himalayan Crystallines, Bhutan: Journal of Metamorphic Geology, v. 15, no. 5, p. 593–612, https://doi.org/10.1111/j.1525-1314.1997.tb00638.x.

DeCelles, P.G., Gehrels, G.E., Quade, J., and Ojha, T.P., 1998, Eocene–early Miocene foreland basin development and the history of Himalayan thrusting, western and central Nepal: Tectonics, v. 17, no. 5, p. 741–765, https://doi.org/10.1029/98TC02598.

DeCelles, P.G., Gehrels, G.E., Quade, J., LaReau, B., and Spurlin, M., 2000, Tectonic implications of U-Pb zircon ages of the Himalayan orogenic belt in Nepal: Science, v. 288, no. 5465, p. 497–499, https://doi.org/10.1126/science.288.5465.497.

DeCelles, P.G., Robinson, D.M., Quade, J., Ojha, T.P., Garzione, C.N., Copeland, P., and Upreti, B.N., 2001, Stratigraphy, structure, and tectonic evolution of the Himalayan fold-thrust belt in western Nepal: Tectonics, v. 20, no. 4, p. 487–509, https://doi.org/10.1029/2000TC001226.

DeCelles, P.G., Carrapa, B., Gehrels, G.E., Chakraborty, T., and Ghosh, P., 2016, Along-strike continuity of structure, stratigraphy, and kinematic history in the Himalayan thrust belt: The view from Northeastern India: Tectonics, v. 35, no. 12, p. 2995–3027, https://doi.org/10.1002/2016TC004298.

Dewey, J.F., Shackleton, R.M., Chengfa, C., and Yiyin, S., 1988, The tectonic evolution of the Tibetan Plateau: Philosophical Transactions of the Royal Society of London A: Mathematical, Physical and Engineering Sciences, v. 327, no. 1594, p. 379–413, https://doi.org/10.1098/rsta.1988.0135.

Dikshitulu, G.R., Pandey, B.K., Krishna, V., and Raju, R.D., 1995, Rb-Sr systematics of granitoids of the central gneissic complex, Arunachal Himalaya: Implications on tectonism, stratigraphy and source: Geological Society of India Publications, v. 45, no. 1, p. 51–56.

Ding, L., Zhong, D., Yin, A., Kapp, P., and Harrison, T.M., 2001, Cenozoic structural and metamorphic evolution of the eastern Himalayan syntaxis (Namche Barwa): Earth and Planetary Science Letters, v. 192, no. 3, p. 423–438, https://doi.org/10.1016/S0012-821X(01)00463-0.

Ding, L., Kapp, P., Zhong, D., and Deng, W., 2003, Cenozoic volcanism in Tibet: Evidence for a transition from oceanic to continental subduction: Journal of Petrology, v. 44, no. 10, p. 1833–1865, https://doi.org/10.1093/petrology/egg061.

Ding, L., Kapp, P., and Wan, X., 2005, Paleocene–Eocene record of ophiolite obduction and initial India-Asia collision, south central Tibet: Tectonics, v. 24, TC3001, https://doi.org/10.1029/2004TC001729.

Dong, X., Zhang, Z., Liu, F., Wang, W., Yu, F., and Shen, K., 2011, Zircon U-Pb geochronology of the Nyainqêntanglha Group from the Lhasa terrane: New constraints on the Triassic orogeny of the south Tibet: Journal of Asian Earth Sciences, v. 42, no. 4, p. 732–739.

Dubois-Côté, V., Hébert, R., Dupuis, C., Wang, C.S., Li, Y.L., and Dostal, J., 2005, Petrological and geochemical evidence for the origin of the Yarlung Zangbo ophiolites, southern Tibet: Chemical Geology, v. 214, no. 3, p. 265–286, https://doi.org/10.1016/j.chemgeo.2004.10.004.

Dupuis, C., Hébert, R., Dubois-Côté, V., Wang, C.S., Li, Y.L., and Li, Z.J., 2005, Petrology and geochemistry of mafic rocks from mélange and flysch units adjacent to the Yarlung Zangbo Suture Zone, southern Tibet: Chemical Geology, v. 214, no. 3, p. 287–308, https://doi.org/10.1016/j.chemgeo.2004.10.005.

Dürr, S.B., 1996, Provenance of Xigaze fore-arc basin clastic rocks (Cretaceous, south Tibet): Geological Society of America Bulletin, v. 108, no. 6, p. 669–684, https://doi.org/10.1130/0016-7606(1996)108<0669:POXFAB>2.3.CO;2.

Edwards, M.A., and Harrison, T.M., 1997, When did the roof collapse?: Late Miocene north-south extension in the high Himalaya revealed by Th-Pb monazite dating of the Khula Kangri

granite: Geology, v. 25, no. 6, p. 543–546, https://doi.org/10.1130/0091-7613(1997)025<0543:WDTRCL>2.3.CO;2.
Edwards, M.A., Kidd, W.S., Li, J., Yue, Y., and Clark, M., 1996, Multi-stage development of the southern Tibet detachment system near Khula Kangri: New data from Gonto La: Tectonophysics, v. 260, no. 1–3, p. 1–19, https://doi.org/10.1016/0040-1951(96)00073-X.
Edwards, M.A., Pêcher, A., Kidd, W.S.F., Burchfiel, B.C., and Royden, L.H., 1999, Southern Tibet Detachment System at Khula Kangri, Eastern Himalaya: A Large-Area, Shallow Detachment Stretching into Bhutan?: The Journal of Geology, v. 107, no. 5, p. 623–631, https://doi.org/10.1086/314366.
Einsele, G., et al., 1994, The Xigaze forearc basin: Evolution and facies architecture (Cretaceous, Tibet): Sedimentary Geology, v. 90, no. 1, p. 1–32, https://doi.org/10.1016/0037-0738(94)90014-0.
England, P., and Houseman, G., 1986, Finite strain calculations of continental deformation: 2. Comparison with the India-Asia collision zone: Journal of Geophysical Research, v. 91, no. B3, p. 3664–3676, https://doi.org/10.1029/JB091iB03p03664.
England, P., and Molnar, P., 1990, Right-lateral shear and rotation as the explanation for strike-slip faulting in eastern Tibet: Nature, v. 344, no. 6262, p. 140–142, https://doi.org/10.1038/344140a0.
Gansser, A., 1964, Geology of the Himalayas: New York, Wiley Interscience, 289 p.
Gansser, A., 1983, Geology of the Bhutan Himalaya: Basel, Birkhauser Verlag, 181 p.
Garzanti, E., and Van Haver, T., 1988, The Indus clastics: Forearc basin sedimentation in the Ladakh Himalaya (India): Sedimentary Geology, v. 59, no. 3–4, p. 237–249, https://doi.org/10.1016/0037-0738(88)90078-4.
Gehrels, G., Kapp, P., DeCelles, P., Pullen, A., Blakey, R., Weislogel, A., Ding, L., Guynn, J., Martin, A., McQuarrie, N., and Yin, A., 2011, Detrital zircon geochronology of pre-Tertiary strata in the Tibetan-Himalayan orogen: Tectonics, v. 30, https://doi.org/10.1029/2011TC002868.
Girardeau, J., et al., 1984, Tectonic environment and geodynamic significance of the Neo-Cimmerian Donqiao ophiolite, Bangong-Nujiang suture zone, Tibet: Nature, v. 307, p. 27–31, https://doi.org/10.1038/307027a0.
Goswami, T.K., 2008, Implications of geochemical signatures in the Trans-Himalayan Lohit batholith, Arunachal Pradesh, India: Himalayan: Journal of Science, v. 5, no. 7, p. 53.
Goswami, T.K., 2011, Collision induces deformation of the Trans Himalayan Lohit Batholith, Arunachal Pradesh, India: Memoir, Geological Society of India, v. 77, v. 19–31.
Goswami, T.K., 2013a, Geodynamic significance of leucogranite intrusions in the Lohit batholith near Walong, eastern Arunachal Pradesh, India: Current Science, v. 104, no. 2, p. 229.
Goswami, T.K., 2013b, Subduction Related Magmatism: Constrains from the REE Pattern in the Lohit Batholith, Arunachal Pradesh, India: Geosciences, v. 3, no. 4, p. 128–141.
Grujic, D., Casey, M., Davidson, C., Hollister, L.S., Kündig, R., Pavlis, T., and Schmid, S., 1996, Ductile extrusion of the Higher Himalayan Crystalline in Bhutan: Evidence from quartz microfabrics: Tectonophysics, v. 260, no. 1, p. 21–43, https://doi.org/10.1016/0040-1951(96)00074-1.
Grujic, D., Hollister, L.S., and Parrish, R.R., 2002, Himalayan metamorphic sequence as an orogenic channel: Insight from Bhutan: Earth and Planetary Science Letters, v. 198, no. 1, p. 177–191, https://doi.org/10.1016/S0012-821X(02)00482-X.
Guan, Q., Zhu, D.C., Zhao, Z.D., Dong, G.C., Zhang, L.L., Li, X.W., Liu, M., Mo, X.X., Liu, Y.S., and Yuan, H.L., 2012, Crustal thickening prior to 38 Ma in southern Tibet: Evidence from lower crust-derived adakitic magmatism in the Gangdese Batholith: Gondwana Research, v. 21, no. 1, p. 88–99, https://doi.org/10.1016/j.gr.2011.07.004.
Gupta, A.D., and Biswas, A.K., 2000, Geology of Assam: Geological Society of India Publications, v. 2, no. 1, p. 169.
Gururajan, N.S., and Choudhuri, B.K., 2003, Geology and tectonic history of the Lohit valley, Eastern Arunachal Pradesh, India: Journal of Asian Earth Sciences, v. 21, no. 7, p. 731–741, https://doi.org/10.1016/S1367-9120(02)00040-8.
Guynn, J., Kapp, P., Gehrels, G.E., and Ding, L., 2012, U-Pb geochronology of basement rocks in central Tibet and paleogeographic implications: Journal of Asian Earth Sciences, v. 43, no. 1, p. 23–50, https://doi.org/10.1016/j.jseaes.2011.09.003.
Haproff, P.J., Zuza, A.V., and Yin, A., 2018, West-directed thrusting south of the eastern Himalayan syntaxis indicates clockwise crustal flow at the indenter corner during the India-Asia collision: Tectonophysics, v. 722, p. 277–285, https://doi.org/10.1016/j.tecto.2017.11.001.
Haq, S.S.B., and Davis, D., 1997, Oblique convergence and the lobate mountain belts of western Pakistan: Geology, v. 25, no. 1, p. 23–26, https://doi.org/10.1130/0091-7613(1997)025<0023:OCATLM>2.3.CO;2.
Harrison, T.M., and Wielicki, M.M., 2016, From the Hadean to the Himalaya: 4.4 Ga of felsic terrestrial magmatism: The American Mineralogist, v. 101, no. 6, p. 1348–1359, https://doi.org/10.2138/am-2016-5516.
Harrison, T.M., Copeland, P., Kidd, W.S.F., and Yin, A., 1992, Raising Tibet: Science, v. 255, p. 1663–1670, https://doi.org/10.1126/science.255.5052.1663.
Harrison, T.M., Yin, A., Grove, M., Lovera, O.M., Ryerson, F.J., and Zhou, X., 2000, The Zedong Window: A record of superposed Tertiary convergence in southeastern Tibet: Journal of Geophysical Research. Solid Earth, v. 105, no. B8, p. 19,211–19,230, https://doi.org/10.1029/2000JB900078.
Hébert, R., Bezard, R., Guilmette, C., Dostal, J., Wang, C.S., and Liu, Z.F., 2012, The Indus–Yarlung Zangbo ophiolites from Nanga Parbat to Namche Barwa syntaxes, southern Tibet: First synthesis of petrology, geochemistry, and geochronology with incidences on geodynamic reconstructions of Neo-Tethys: Gondwana Research, v. 22, no. 2, p. 377–397, https://doi.org/10.1016/j.gr.2011.10.013.
Heim, A., and Gansser, A., 1939, Central Himalaya: Delhi, Hindustan Publishing.
Hodges, K.V., 2000, Tectonics of the Himalaya and southern Tibet from two perspectives: Geological Society of America Bulletin, v. 112, no. 3, p. 324–350, https://doi.org/10.1130/0016-7606(2000)112<324:TOTHAS>2.0.CO;2.
Honegger, K., Dietrich, V., Frank, W., Gansser, A., Thöni, M., and Trommsdorff, V., 1982, Magmatism and metamorphism in the Ladakh Himalayas (the Indus-Tsangpo suture zone): Earth and Planetary Science Letters, v. 60, no. 2, p. 253–292, https://doi.org/10.1016/0012-821X(82)90007-3.
Hsü, K., et al., 1995, Tectonic evolution of the Tibetan Plateau: A working hypothesis based on the archipelago model of orogenesis: International Geology Review, v. 37, p. 473–508, https://doi.org/10.1080/00206819509465414.
Hu, X., Wang, J., Boudagher-Fadel, M., Garzanti, E., and An, W., 2015, New insights into the timing of the India-Asia collision from the Paleogene Quxia and Jialazi Formations of the Xigaze Forearc Basin, South Tibet: Gondwana Research, v. 32, p. 76–92, https://doi.org/10.1016/j.gr.2015.02.007.
Huyghe, P., Galy, A., Mugnier, J.L., and France-Lanord, C., 2001, Propagation of the thrust system and erosion in the Lesser Himalaya: Geochemical and sedimentological evidence: Geology, v. 29, no. 11, p. 1007–1010, https://doi.org/10.1130/0091-7613(2001)029<1007:POTTSA>2.0.CO;2.
Jangpangi, B.S., 1974, Stratigraphy and tectonics of parts of eastern Bhutan: Himalayan Geology, v. 4, p. 117–136.
Ji, W.Q., Wu, F.Y., Chung, S.L., Li, J.X., and Liu, C.Z., 2009, Zircon U-Pb geochronology and Hf isotopic constraints on petrogenesis of the Gangdese batholith, southern Tibet: Chemical Geology, v. 262, no. 3, p. 229–245, https://doi.org/10.1016/j.chemgeo.2009.01.020.
Johnson, D.M., Hooper, P.R., and Conrey, R.M., 1999, XRF Analysis of Rocks and Minerals for Major and Trace Elements on a Single Low Dilution Li-tetraborate Fused Bead: GeoAnalytical Lab, Washington State University, Advances in X-ray Analysis, v. 41, p. 843–867.
Kapp, P., Murphy, M.A., Yin, A., Harrison, T.M., Ding, L., and Guo, J., 2003, Mesozoic and Cenozoic tectonic evolution of the Shiquanhe area of western Tibet: Tectonics, v. 22, no. 4, https://doi.org/10.1029/2001TC001332.
Kistler, R.W., and Ross, D.C., 1990, A strontium isotopic study of plutons and associated rocks of the southern Sierra Nevada vicinity, California: U.S. Government Printing Office, Books and Open-File Reports Section, U.S. Geological Survey Bulletin, no. 1920, 20 p.
Kumar, G., 1997, Geology of Arunachal Pradesh: Bangalore, Geological Society of India, p. 217.
Kylander-Clark, A.R., Hacker, B.R., and Cottle, J.M., 2013, Laser-ablation split-stream ICP petrochronology: Chemical Geology, v. 345, p. 99–112, https://doi.org/10.1016/j.chemgeo.2013.02.019.
Laskowski, A.K., Kapp, P., Vervoort, J.D., and Ding, L., 2016, High-pressure Tethyan Himalaya rocks along the India-Asia suture zone in southern Tibet: Lithosphere, v. 8, no. 5, p. 574–582, https://doi.org/10.1130/L544.1.
Leary, R.J., DeCelles, P.G., Quade, J., Gehrels, G.E., and Waanders, G., 2016, The Liuqu Conglomerate, southern Tibet: Early Miocene basin development related to deformation within the Great Counter Thrust system: Lithosphere, v. 8, no. 5, p. 427–450, https://doi.org/10.1130/L542.1.
Le Bas, M.J., Le Maitre, R.W., Streckeisen, A., and Zanettin, B., 1986, A chemical classification of volcanic rocks based on the total alkali-silica diagram: Journal of Petrology, v. 27, no. 3, p. 745–750, https://doi.org/10.1093/petrology/27.3.745.
Lee, H.Y., Chung, S.L., Lo, C.H., Ji, J., Lee, T.Y., Qian, Q., and Zhang, Q., 2009, Eocene Neotethyan slab breakoff in southern Tibet inferred from the Linzizong volcanic record: Tectonophysics, v. 477, no. 1, p. 20–35, https://doi.org/10.1016/j.tecto.2009.02.031.
Lee, H.Y., Chung, S.L., and Yang, H.M., 2016, Late Cenozoic volcanism in central Myanmar: Geochemical characteristics and geodynamic significance: Lithos, v. 245, p. 174–190, https://doi.org/10.1016/j.lithos.2015.09.018.
Le Fort, P., 1975, Himalayas: The collided range: Present knowledge of the continental arc: American Journal of Science, v. 275, p. 1–44.
Le Fort, P., 1996, Evolution of the Himalaya, *in* Yin, A., and Harrison, T.M., eds., The Tectonic Evolution of Asia: New York, Cambridge University Press, p. 95–106.

Lin, T.H., Chung, S.L., Kumar, A., Wu, F.Y., Chiu, H.Y., and Lin, I., 2013, Linking a prolonged Neo-Tethyan magmatic arc in South Asia: Zircon U-Pb and Hf isotopic constraints from the Lohit Batholith, NE India: Terra Nova, v. 25, no. 6, p. 453–458, https://doi.org/10.1111/ter.12056.
Liu, D.L., Shi, R.D., Ding, L., and Zou, H.B., 2018, Late Cretaceous transition from subduction to collision along the Bangong-Nujiang Tethys: New volcanic constraints from central Tibet: Lithos, v. 296, p. 452–470, https://doi.org/10.1016/j.lithos.2017.11.012.
Long, S., and McQuarrie, N., 2010, Placing limits on channel flow: Insights from the Bhutan Himalaya: Earth and Planetary Science Letters, v. 290, no. 3, p. 375–390, https://doi.org/10.1016/j.epsl.2009.12.033.
Long, S., McQuarrie, N., Tobgay, T., and Grujic, D., 2011a, Geometry and crustal shortening of the Himalayan fold-thrust belt, eastern and central Bhutan: Geological Society of America Bulletin, v. 123, p. 1427–1447, https://doi.org/10.1130/B30203.1.
Long, S., McQuarrie, N., Tobgay, T., and Hawthorne, J., 2011b, Quantifying internal strain and deformation temperature in the eastern Himalaya, Bhutan: Implications for the evolution of strain in thrust sheets: Journal of Structural Geology, v. 33, no. 4, p. 579–608, https://doi.org/10.1016/j.jsg.2010.12.011.
Long, S., McQuarrie, N., Tobgay, T., Rose, C., Gehrels, G., and Grujic, D., 2011c, Tectonostratigraphy of the Lesser Himalaya of Bhutan: Implications for the along-strike stratigraphic continuity of the northern Indian margin: Geological Society of America Bulletin, v. 123, no. 7–8, p. 1406–1426, https://doi.org/10.1130/B30202.1.
Ludwig, K.R., 1991, ISOPLOT: a plotting and regression program for radiogenic-isotope data: U.S. Geological Survey Open-File Report 91-445, https://doi.org/10.3133/ofr91445.
Malpas, J., Zhou, M.F., Robinson, P.T., and Reynolds, P.H., 2003, Geochemical and geochronological constraints on the origin and emplacement of the Yarlung Zangbo ophiolites, Southern Tibet: Geological Society of London, Special Publications, v. 218, no. 1, p. 191–206, https://doi.org/10.1144/GSL.SP.2003.218.01.11.
McDermid, I.R., Aitchison, J.C., Davis, A.M., Harrison, T.M., and Grove, M., 2002, The Zedong terrane: A Late Jurassic intra-oceanic magmatic arc within the Yarlung-Tsangpo suture zone, southeastern Tibet: Chemical Geology, v. 187, no. 3, p. 267–277, https://doi.org/10.1016/S0009-2541(02)00040-2.
McQuarrie, N., Robinson, D., Long, S., Tobgay, T., Grujic, D., Gehrels, G., and Ducea, M., 2008, Preliminary stratigraphic and structural architecture of Bhutan: Implications for the along strike architecture of the Himalayan system: Earth and Planetary Science Letters, v. 272, no. 1, p. 105–117, https://doi.org/10.1016/j.epsl.2008.04.030.
Misra, D.K., 2009, Litho-tectonic sequence and their regional correlation along the Lohit and Dibang valleys, eastern Arunachal Pradesh: Journal of the Geological Society of India, v. 73, no. 2, p. 213–219, https://doi.org/10.1007/s12594-009-0077-x.
Misra, D.K., and Singh, T., 2002, Tectonic setting and neotectonic features along the Eastern Syntaxial Bend (Lohit and Dibang), Arunachal Himalaya: Aspects of Geology and Environment of the Himalaya: Gyanodaya Prakashan, Nainital, India, p. 19–40.
Mitchell, A.H.G., 1993, Cretaceous–Cenozoic tectonic events in the western Myanmar (Burma)–Assam region: Journal of the Geological Society of London, v. 150, no. 6, p. 1089–1102, https://doi.org/10.1144/gsjgs.150.6.1089.
Mitchell, A.H.G., Chung, S.L., Oo, T., Lin, T.H., and Hung, C.H., 2012, Zircon U-Pb ages in Myanmar: Magmatic-metamorphic events and the closure of a neo-Tethys ocean?: Journal of Asian Earth Sciences, v. 56, p. 1–23, https://doi.org/10.1016/j.jseaes.2012.04.019.
Nandini, P., and Thakur, S.S., 2011, Metamorphic evolution of the Lesser Himalayan Crystalline Sequence, Siyom Valley, NE Himalaya, India: Journal of Asian Earth Sciences, v. 40, no. 5, p. 1089–1100, https://doi.org/10.1016/j.jseaes.2010.12.005.
Nandy, D.R., 1973, Geology and structural lineaments of the Lohit Himalaya (Arunachal Pradesh) and adjoining area, *in* Gupta, H.K., ed., Seminar on Geodynamics of the Himalayan Region: Hyderabad, National Geophysical Research Institute, p. 167–172.
Ni, J.F., Guzman-Speziale, M., Bevis, M., Holt, W.E., Wallace, T.C., and Seager, W.R., 1989, Accretionary tectonics of Burma and the three-dimensional geometry of the Burma subduction zone: Geology, v. 17, p. 68–71, https://doi.org/10.1130/0091-7613(1989)017<0068:ATOBAT>2.3.CO;2.
Ningthoujam, P.S., Dubey, C.S., Lolee, L.K., Shukla, D.P., Naorem, S.S., and Singh, S.K., 2015, Tectonic studies and crustal shortening across easternmost Arunachal Himalaya: Journal of Asian Earth Sciences, v. 111, p. 339–349, https://doi.org/10.1016/j.jseaes.2015.07.003.
Orme, D.A., Carrapa, B., and Kapp, P., 2015, Sedimentology, provenance and geochronology of the Upper Cretaceous–Lower Eocene western Xigaze forearc basin, southern Tibet: Basin Research, v. 27, no. 4, p. 387–411, https://doi.org/10.1111/bre.12080.
Paces, J.B., and Miller Jr, J.D., 1993, Precise U-Pb ages of Duluth complex and related mafic intrusions, northeastern Minnesota: Geochronological insights to physical, petrogenetic, paleomagnetic, and tectonomagmatic processes associated with the 1.1 Ga midcontinent rift system: Journal of Geophysical Research. Solid Earth, v. 98, p. 13997–14013.
Parrish, R.R., and Hodges, V., 1996, Isotopic constraints on the age and provenance of the Lesser and Greater Himalayan sequences, Nepalese Himalaya: Geological Society of America Bulletin, v. 108, no. 7, p. 904–911, https://doi.org/10.1130/0016-7606(1996)108<0904:ICOTAA>2.3.CO;2.
Pearce, J.A., 1982, Trace element characteristics of lavas from destructive plate boundaries, *in* Thorpe, R.S., ed., Andesites: Orogenic Andesites and Related Rocks: Chichester, UK, John Wiley and Sons, p. 525–548.
Pearce, J.A., Harris, N.B., and Tindle, A.G., 1984, Trace element discrimination diagrams for the tectonic interpretation of granitic rocks: Journal of Petrology, v. 25, no. 4, p. 956–983, https://doi.org/10.1093/petrology/25.4.956.
Quidelleur, X., Grove, M., Lovera, O.M., Harrison, T.M., and Yin, A., 1997, Thermal evolution and slip history of the Renbu-Zedong Thrust, southeastern Tibet: Journal of Geophysical Research, v. 102, p. 2659–2680, https://doi.org/10.1029/96JD02483.
Richards, A., Parrish, R., Harris, N., Argles, T., and Zhang, L., 2006, Correlation of lithotectonic units across the eastern Himalaya, Bhutan: Geology, v. 34, no. 5, p. 341–344, https://doi.org/10.1130/G22169.1.
Robinson, D.M., DeCelles, P.G., Patchett, P.J., and Garzione, C.N., 2001, The kinematic evolution of the Nepalese Himalaya interpreted from Nd isotopes: Earth and Planetary Science Letters, v. 192, no. 4, p. 507–521, https://doi.org/10.1016/S0012-821X(01)00451-4.
Royden, L.H., Burchfiel, B.C., King, R.W., Wang, E., Chen, Z., Shen, F., and Liu, Y., 1997, Surface deformation and lower crustal flow in eastern Tibet: Science, v. 276, p. 788–790, https://doi.org/10.1126/science.276.5313.788.
Sarma, K.P., Nandy, S., Devi, N.R., and Konwar, P., 2009, Is Mishmi Block a Tectonic Roof? Some Observations, *in* Kumar, S., ed., Magmatism, Tectonism and Mineralization: New Delhi, India, Macmilan Publishers India Ltd., p. 167–178.
Sarma, K.P., Nandy, S., and Mazumdar, N., 2012, Structural studies of the Mishmi block in parts of Dibang Valley of Arunachal Himalaya, Northeast India: International Journal of Geology: Earth and Environmental Sciences, v. 2, no. 3, p. 43–56.
Schärer, U., Xu, R.H., and Allègre, C.J., 1984, U-Pb geochronology of Gangdese (Transhimalaya) plutonism in the Lhasa-Xigaze region, Tibet: Earth and Planetary Science Letters, v. 69, no. 2, p. 311–320, https://doi.org/10.1016/0012-821X(84)90190-0.
Schmitt, A.K., Grove, M., Harrison, T.M., Lovera, O., Hulen, J., and Walters, M., 2003a, The Geysers-Cobb Mountain Magma System, California (Part 1): U-Pb zircon ages of volcanic rocks, conditions of zircon crystallization and magma residence times: Geochimica et Cosmochimica Acta, v. 67, no. 18, p. 3423–3442, https://doi.org/10.1016/S0016-7037(03)00140-6.
Schmitt, A.K., Grove, M., Harrison, T.M., Lovera, O., Hulen, J., and Walters, M., 2003b, The Geysers-Cobb Mountain Magma System, California (Part 2): Timescales of pluton emplacement and implications for its thermal history: Geochimica et Cosmochimica Acta, v. 67, no. 18, p. 3443–3458, https://doi.org/10.1016/S0016-7037(03)00126-1.
Shand, S.J., 1943, Eruptive Rocks: Their Genesis, Composition, Classification, and Their Relation to Ore Deposits, with a Chapter on Meteorites (Revised Second Edition): New York, Wiley, 444 p.
Sharma, K.K., Choubey, V.M., and Chatti, H.R., 1991, Geological setting of the ophiolites and magmatic arc of the Lohit Himalaya (Arunachal Pradesh), India with special reference to their petrochemistry: Physics and Chemistry of the Earth, v. 18, p. 277–292, https://doi.org/10.1016/0079-1946(91)90005-Z.
Sharma, R., and Sarma, K.P., 2013, Microstructural study and strain history of Mesoproterozoic augen gneiss of Lohit District, Arunachal Himalaya, India: International Journal of Geology, Earth and Environment Sciences, v. 3, no. 2, p. 68–76.
Shervais, J.W., 1982, Ti-V plots and the petrogenesis of modern and ophiolitic lavas: Earth and Planetary Science Letters, v. 59, no. 1, p. 101–118, https://doi.org/10.1016/0012-821X(82)90120-0.
Singh, B., 1993, Geological set up of a part of the Ladakh Granitoid Complex: Ladakh Himalaya: Journal of Himalayan Geology, v. 4, no. 1, p. 57–62.
Singh, S., and Chowdhury, P.K., 1990, An outline of the geological framework of the Arunachal Himalaya: Journal of Himalayan Geology, v. 1, no. 2, p. 189–197.
Srivastava, R.K., and Sinha, A.K., 2004a, Geochemistry of Early Cretaceous alkaline ultramafic-mafic complex from Jasra, Karbi Anglong, Shillong plateau, northeastern India: Gondwana Research, v. 7, no. 2, p. 549–561, https://doi.org/10.1016/S1342-937X(05)70805-4.
Srivastava, R.K., and Sinha, A.K., 2004b, Early Cretaceous Sung Valley ultramafic-alkaline-carbonatite complex, Shillong Plateau, Northeastern India: petrological and genetic significance: Mineralogy and Petrology, v. 80, no. 3, p. 241–263, https://doi.org/10.1007/s00710-003-0025-1.
Srivastava, R.K., Heaman, L.M., Sinha, A.K., and Shihua, S., 2005, Emplacement age and isotope geochemistry of Sung Valley alkaline-carbonatite complex, Shillong Plateau, northeastern

India: Implications for primary carbonate melt and genesis of the associated silicate rocks: Lithos, v. 81, no. 1, p. 33–54, https://doi.org/10.1016/j.lithos.2004.09.017.
Stacey, J.S., and Kramers, J.D., 1975, Approximation of terrestrial lead isotope evolution by a two-stage model: Earth and Planetary Science Letters, v. 26, no. 2, p. 207–221, https://doi.org/10.1016/0012-821X(75)90088-6.
Swapp, S.M., and Hollister, L.S., 1991, Inverted metamorphism within the Tibetan slab of Bhutan: Evidence for a tectonically transported heat-source: Canadian Mineralogist, v. 29, no. 4, p. 1019–1041.
Tapponnier, P., Mattauer, M., Proust, F., and Cassaigneau, C., 1981, Mesozoic ophiolites, sutures, and large-scale tectonic movements in Afghanistan: Earth and Planetary Science Letters, v. 52, no. 2, p. 355–371, https://doi.org/10.1016/0012-821X(81)90189-8.
Tapponnier, P., Peltzer, G., Le Dain, A.Y., Armijo, R., and Cobbold, P., 1982, Propagating extrusion tectonics in Asia: New insights from simple experiments with plasticine: Geology, v. 10, p. 611–616, https://doi.org/10.1130/0091-7613(1982)10<611:PETIAN>2.0.CO;2.
Tapponnier, P., Zhiqin, X., Roger, F., Meyer, B., Arnaud, N., Wittlinger, G., and Jingsui, Y., 2001, Oblique stepwise rise and growth of the Tibet Plateau: Science, v. 294, no. 5547, p. 1671–1677, https://doi.org/10.1126/science.105978.
Tewari, V.C., Lokho, K., Kumar, K., and Siddaiah, N.S., 2010, Late Cretaceous–Paleogene basin architecture and evolution of the Shillong shelf sedimentation, Meghalaya, Northeast India: Journal of the Indian Geological Congress, v. 2, no. 2, p. 61–73.
Thakur, V.C., and Jain, A.K., 1975, Some observations of deformation and metamorphism in the rocks of some parts of Mishmi Hills, Lohit district, (NEFA), Arunachal Pradesh: Himalayan Geology, v. 5, p. 339–364.
Wadia, D.N., 1931, The syntaxis of the northwest Himalaya: Its rocks, tectonics and orogeny: Records of the Geological Survey of India, v. 65, no. 2, p. 189–220.
Wang, C., Li, X., Liu, Z., Li, Y., Jansa, L., Dai, J., and Wei, Y., 2012, Revision of the Cretaceous–Paleogene stratigraphic framework, facies architecture and provenance of the Xigaze forearc basin along the Yarlung Zangbo suture zone: Gondwana Research, v. 22, no. 2, p. 415–433, https://doi.org/10.1016/j.gr.2011.09.014.
Wang, C., Ding, L., Zhang, L.Y., Kapp, P., Pullen, A., and Yue, Y.H., 2016, Petrogenesis of Middle–Late Triassic volcanic rocks from the Gangdese belt, southern Lhasa terrane: Implications for early subduction of Neo-Tethyan oceanic lithosphere: Lithos, v. 262, p. 320–333, https://doi.org/10.1016/j.lithos.2016.07.021.
Wang, Y., Zhang, L., Cawood, P.A., Ma, L., Fan, W., Zhang, A., Zhang, Y., and Bi, X., 2014, Eocene supra-subduction zone mafic magmatism in the Sibumasu Block of SW Yunnan: Implications for Neotethyan subduction and India-Asia collision: Lithos, v. 206, p. 384–399, https://doi.org/10.1016/j.lithos.2014.08.012.
Webb, A.A.G., 2013, Preliminary balanced palinspastic reconstruction of Cenozoic deformation across the Himachal Himalaya (northwestern India): Geosphere, v. 9, no. 3, p. 572–587, https://doi.org/10.1130/GES00787.1.
Webb, A.A.G., Yin, A., and Dubey, C.S., 2013, U-Pb zircon geochronology of major lithologic units in the eastern Himalaya: Implications for the origin and assembly of Himalayan rocks: Geological Society of America Bulletin, v. 125, no. 3–4, p. 499–522, https://doi.org/10.1130/B30626.1.
Webb, A.A.G., Guo, H., Clift, P.D., Husson, L., Müller, T., Costantino, D., Yin, A., Xu, Z., Cao, H., Wang, Q., 2017, The Himalaya in 3D: Slab dynamics controlled mountain building and monsoon intensification: Lithosphere, v. 9, p. 637–651.
Wen, D.R., Liu, D., Chung, S.L., Chu, M.F., Ji, J., Zhang, Q., Song, B., Lee, T.Y., Yeh, M.W., and Lo, C.H., 2008, Zircon SHRIMP U-Pb ages of the Gangdese Batholith and implications for Neotethyan subduction in southern Tibet: Chemical Geology, v. 252, no. 3, p. 191–201, https://doi.org/10.1016/j.chemgeo.2008.03.003.
Wiedenbeck, M., Allé, P., Corfu, F., Griffin, W.L., Meier, M., Oberli, F., Von Quadt, A., Roddick, J.C., and Spiegel, W., 1995, Three natural zircon standards for U-Th-Pb, Lu-Hf, trace element and REE analyses: Geostandards Newsletter, v. 19, no. 1, p. 1–23.
Williams, H., Turner, S., Kelley, S., and Harris, N., 2001, Age and composition of dikes in Southern Tibet: New constraints on the timing of east-west extension and its relationship to postcollisional volcanism: Geology, v. 29, no. 4, p. 339–342, https://doi.org/10.1130/0091-7613(2001)029<0339:AACODI>2.0.CO;2.
Wu, C., Nelson, K.D., Wortman, G., Samson, S.D., Yue, Y., Li, J., Kidd, W.S.F., and Edwards, M.A., 1998, Yadong cross structure and South Tibetan Detachment in the east central Himalaya (89–90): Tectonics, v. 17, no. 1, p. 28–45, https://doi.org/10.1029/97TC03386.
Xu, W.C., Zhang, H.F., Harris, N., Guo, L., Pan, F.B., and Wang, S., 2013, Geochronology and geochemistry of Mesoproterozoic granitoids in the Lhasa terrane, south Tibet: Implications for the early evolution of Lhasa terrane: Precambrian Research, v. 236, p. 46–58, https://doi.org/10.1016/j.precamres.2013.07.016.
Yin, A., 2006, Cenozoic tectonic evolution of the Himalayan orogen as constrained by along-strike variation of structural geometry, exhumation history, and foreland sedimentation: Earth-Science Reviews, v. 76, no. 1, p. 1–131, https://doi.org/10.1016/j.earscirev.2005.05.004.
Yin, A., 2010, Cenozoic tectonic evolution of Asia: A preliminary synthesis: Tectonophysics, v. 488, no. 1, p. 293–325, https://doi.org/10.1016/j.tecto.2009.06.002.
Yin, A., and Harrison, T.M., 2000, Geologic Evolution of the Himalayan-Tibetan Orogen: Annual Review of Earth and Planetary Sciences, v. 28, p. 211–280, https://doi.org/10.1146/annurev.earth.28.1.211.
Yin, A., Harrison, T.M., Ryerson, F.J., Wenji, C., Kidd, W.S.F., and Copeland, P., 1994, Tertiary structural evolution of the Gangdese thrust system, southeastern Tibet: Journal of Geophysical Research. Solid Earth, v. 99, no. B9, p. 18,175–18,201, https://doi.org/10.1029/94JB00504.
Yin, A., Harrison, T.M., Murphy, M.A., Grove, M., Nie, S., Ryerson, F.J., Feng, W.X., and Le, C.Z., 1999, Tertiary deformation history of southeastern and southwestern Tibet during the Indo-Asian collision: Geological Society of America Bulletin, v. 111, no. 11, p. 1644–1664, https://doi.org/10.1130/0016-7606(1999)111<1644:TDHOSA>2.3.CO;2.
Yin, A., Dubey, C.S., Kelty, T.K., Gehrels, G.E., Chou, C.Y., Grove, M., and Lovera, O., 2006, Structural evolution of the Arunachal Himalaya and implications for asymmetric development of the Himalayan orogen: Current Science, v. 90, no. 2, p. 195–200.
Yin, A., Dubey, C.S., Webb, A.A.G., Kelty, T.K., Grove, M., Gehrels, G.E., and Burgess, W.P., 2010a, Geologic correlation of the Himalayan orogen and Indian craton: Part 1. Structural geology, U-Pb zircon geochronology, and tectonic evolution of the Shillong Plateau and its neighboring regions in NE India: Geological Society of America Bulletin, v. 122, no. 3–4, p. 336–359, https://doi.org/10.1130/B26460.1.
Yin, A., Dubey, C.S., Kelty, T.K., Webb, A.A.G., Harrison, T.M., Chou, C.Y., and Célérier, J., 2010b, Geologic correlation of the Himalayan orogen and Indian craton: Part 2. Structural geology, geochronology, and tectonic evolution of the Eastern Himalaya: Geological Society of America Bulletin, v. 122, p. 360–395, https://doi.org/10.1130/B26461.1.
Zeiger, K., Gordon, S.M., Long, S.P., Kylander-Clark, A.R.C., Agustsson, K., and Penfold, M., 2015, Timing and conditions of metamorphism and melt crystallization in Greater Himalayan rocks, eastern and central Bhutan: Insight from U-Pb zircon and monazite geochronology and trace-element analyses: Contributions to Mineralogy and Petrology, v. 169, no. 5, https://doi.org/10.1007/s00410-015-1143-6.
Zeng, L., Gao, L.E., Xie, K., and Liu-Zeng, J., 2011, Mid-Eocene high Sr/Y granites in the Northern Himalayan Gneiss Domes: Melting thickened lower continental crust: Earth and Planetary Science Letters, v. 303, no. 3, p. 251–266, https://doi.org/10.1016/j.epsl.2011.01.005.
Zhang, X., et al., 2014, Early Jurassic high-pressure metamorphism of the Amdo terrane, Tibet: Constraints from zircon U-Pb geochronology of mafic granulites: Gondwana Research, v. 26, no. 3, p. 975–985, https://doi.org/10.1016/j.gr.2013.08.003.
Zhou, M.F., Robinson, P.T., Malpas, J., Edwards, S.J., and Qi, L., 2005, REE and PGE geochemical constraints on the formation of dunites in the Luobusa ophiolite, Southern Tibet: Journal of Petrology, v. 46, no. 3, p. 615–639, https://doi.org/10.1093/petrology/egh091.
Zhu, D.C., Pan, G.T., Chung, S.L., Liao, Z.L., Wang, L.Q., and Li, G.M., 2008, SHRIMP zircon age and geochemical constraints on the origin of Lower Jurassic volcanic rocks from the Yeba Formation, southern Gangdese, South Tibet: International Geology Review, v. 50, no. 5, p. 442–471, https://doi.org/10.2747/0020-6814.50.5.442.
Zhu, D.C., Chung, S.L., Mo, X.X., Zhao, Z.D., Niu, Y., Song, B., and Yang, Y.H., 2009a, The 132 Ma Comei-Bunbury large igneous province: Remnants identified in present-day southeastern Tibet and southwestern Australia: Geology, v. 37, no. 7, p. 583–586, https://doi.org/10.1130/G30001A.1.
Zhu, D.C., Zhao, Z.D., Pan, G.T., Lee, H.Y., Kang, Z.Q., Liao, Z.L., Wang, L.Q., Li, G.M., Dong, C., and Liu, B., 2009b, Early cretaceous subduction-related adakite-like rocks of the Gangdese Belt, southern Tibet: Products of slab melting and subsequent melt-peridotite interaction?: Journal of Asian Earth Sciences, v. 34, no. 3, p. 298–309, https://doi.org/10.1016/j.jseaes.2008.05.003.
Zhu, D.C., Zhao, Z.D., Niu, Y., Dilek, Y., and Mo, X.X., 2011, Lhasa terrane in southern Tibet came from Australia: Geology, v. 39, no. 8, p. 727–730, https://doi.org/10.1130/G31895.1.
Zhu, D.C., Zhao, Z.D., Niu, Y., Dilek, Y., Wang, Q., Ji, W.H., Dong, G.C., Sui, Q.L., Liu, Y.S., Yuan, H.L., and Mo, X.X., 2012, Cambrian bimodal volcanism in the Lhasa Terrane, southern Tibet: Record of an early Paleozoic Andean-type magmatic arc in the Australian proto-Tethyan margin: Chemical Geology, v. 328, p. 290–308, https://doi.org/10.1016/j.chemgeo.2011.12.024.
Ziabrev, S., Aitchison, J., Abrajevitch, A., Davis, A., and Luo, H., 2003, Precise radiolarian age constraints on the timing of ophiolite generation and sedimentation in the Dazhuqu terrane, Yarlung-Tsangpo suture zone, Tibet: Journal of the Geological Society of London, v. 160, no. 4, p. 591–599, https://doi.org/10.1144/0016-764902-107.
Zuza, A.V., Wu, C., Wang, Z., Levy, D.A., Li, B., Xiong, X., and Chen, X., 2019, Underthrusting and duplexing beneath the northern Tibetan Plateau and the evolution of the Himalayan-Tibetan orogen: Lithosphere, v. 11, p. 209–231, https://doi.org/10.1130/L1042.1.